Oyahida Khatun: Research details

Title: Dissecting Molecular Interactions Between SARS-CoV-2 and Human Cellular Factors: Mechanisms of Infection, Replication, and Pathogenesis

Introduction: The SARS-CoV-2 virus, the etiological agent of COVID-19, exploits host machinery for its life cycle while evading the immune response. Understanding the molecular interactions between host factors and viral proteins is crucial for comprehending COVID-19 dynamics, including disease progression and transmission. This knowledge is also essential for identifying potential therapeutic targets. To probe into these realms, my research concentration is segmented into two principal projects: identify therapeutic target against SARS-CoV-2 infection and elucidate viral immune evasion mechanism.

Chapters:

I) Identification and characterization of cellular targets for host-directed therapy against SARS-CoV-2.

1.1 Introduction

The COVID-19 pandemic has emerged as the first biggest global public health crisis of the 21st century, affecting more than 775 million people worldwide (https://data.who.int/dashboards/covid19/cases?n=o). Numerous research teams have utilized cutting-edge high-throughput techniques to examine the host responses following viral infections(1-7). These have generated a wealth of OMICS data which holds the key to novel therapeutic strategies and proteins. Comprehending the host response in the upper respiratory tract, the primary site of infection is essential to understanding the pathogenesis of viruses. In order to better understand COVID-19 pathophysiology, several research groups have used nasopharyngeal swabs and BALF to identify changes in transcripts and proteins during infection. These studies have highlighted significantly upregulated genes and biological pathways altered during infection. Our study's objective was to identify genes that are consistently elevated in patients' upper respiratory tracts during SARS-CoV-2 infection and to comprehend the significance of these genes for viral infection and disease progression.

1.2 Objective

Identify significantly upregulated genes at the upper respiratory tract during SARS-CoV-2 infection, explore their potential as candidate for host-directed therapy (HDT) against SARS-CoV-2 infection. Furthermore, we want to explore the combination of this HDT candidate with antivirals directly targeting viral protein or life cycle.

1.3 Materials and Methods

1.3.1 Ethical statement

This research was carried out with permission from Institutional Bio-Safety Committee (Approval Number: IBSC/IISc/ST/17/2020) and Institutional Animal Ethics Committee (Approval Number: IAEC/IISc/ST/784/2020), following the Indian Council of Medical Research and Department of Biotechnology recommendations. All experiments involving infectious SARS-CoV-2 were conducted in the Viral Biosafety level-3 facility at the Indian Institute of Science.

1.3.2 Gene set overlap analysis

A contingency table was used to assess the independence of two lists of genes using the GeneOverlap class of the R package "GeneOverlap". Fisher's exact test was then utilized to determine the statistical significance. Genes selected for additional analysis have a p-value of less than 0.01 for overlap.

1.3.3 Cells and viruses

HEK 293T cells expressing human ACE2 (NR-52511, BEI Resources, NIAID, NIH, RRID: CVCL_A7UK) and VeroE6 cells (CRL-1586, ATCC, RRID:CVCL_0574) were cultured in complete media containing Dulbecco's modified Eagle medium with 10% HI-FBS ,100 IU/ml Penicillin, 100 µg/ml Streptomycin and 0.25µg/ml Amphotericin-B (Penicillin-Streptomycin-Amphotericin B) supplemented with GlutaMAX™. As previously described, SARS-CoV2 (Isolate Hong Kong/VM20001061/2020, NR-52282, BEI Resources, NIAID, NIH) was propagated and titrated in Vero E6 cells using the plaque assay (8).

1.3.4 Cytotoxicity assay

A 96-well cell culture dish with pre-coating using 0.1 mg/mL poly-L-lysine was used to seed HEK-ACE2 cells. The cells were treated in triplicate with 0, 1, 2, and 4 µM Auranofin (A6733, Sigma-Aldrich), after 24 hours of seeding. The AlamarBlueTM Cell Viability Reagent was

used to assess the cytotoxicity of the cells 48 hours after the drug addition, in accordance with the manufacturer's instructions.

1.3.5 Infection in cells

In a poly-L-lysine pre-coated 24-well cell culture dish, HEK-ACE2 cells were seeded and used for infection 24 hours later. For infection in HEK-ACE2, cells were first pretreated for 3 hr with 0, 0.125, 0.25, 0.5, and 1μM Auranofin in quadruplicates. Cells were infected at 0.1 MOI with 100 μl of inoculum in DMEM supplemented with 10% FBS. For infection in VeroE6, in quadruplicates, cells were pretreated with 0 and 1 μM Auranofin for three hours. Cells were infected at 0.001 MOI with 100 μl of inoculum in DMEM supplemented with 2% FBS. Complete media (DMEM with 2% FBS for VeroE6) was added to the cells for both cell lines, restoring the drug's initial dosage. After 48 hours, cells were treated independently for RNA extraction (harvested in TRIzol), western blot analysis, and plaque test.

1.3.6 Western blot

1X PBS was used to wash the cells, and 1X Laemmli buffer was used to lyse them. Cell lysates were separated by a 10% SDS-PAGE gel and were transferred onto a PVDF membrane. Blocking was done for two hours at room temperature with gentle rocking using 5% skimmed milk in 1X PBS containing 0.05% Tween 20 (1X PBST). SARS-CoV / SARS-CoV-2 (COVID-19) spike antibody (180 KDa) (GTX632604, GeneTex, or NR-52947, BEI Resources, NIAID, NIH) was used for the primary antibody incubation, which was carried out overnight (12 hours) at 4°C. The secondary antibody incubation was carried out using Goat Anti-Mouse IgG H&L or Goat Anti-Rabbit IgG H&L for two hours at room temperature with moderate rocking. The Clarity Western ECL Substrate was used to develop the blots. Using a mouse monoclonal antibody to beta Actin [AC-15] (HRP) (ab49900, Abcam), blots were probed for beta-actin (42 KDa).

1.3.7 Plaque assay

The plaque test was used as previously reported (8) to quantify the amounts of infectious viruses. VeroE6 cells were seeded in 6-well cell culture trays and allowed to grow to complete confluency. Cells incubated with dilutions of cell culture supernatants in 200 μL complete DMEM for 1 hr at 37°C. After removing the virus inoculum, cells were covered with DMEM supplemented with 0.8% agarose and 2% FBS. Following a 48-hour incubation period, cells were fixed using 4% formalin, and plaques were made visible using a crystal violet stain.

1.3.8 Tissue-culture infectious dose 50 ($TCID_{50}$)

A poly-L-lysine pre-coated 96-well cell culture dish was used to seed HEK-ACE2 cells, which were then used for infection 24 hours later. After a three-hour pretreatment with 1 μM Auranofin, cells were infected with SARS-CoV-2 with two-fold serial dilutions of SARS-CoV-2 starting at 0.1 MOI. Ten wells were used for each condition. After 48 hours of incubation, the presence or lack of cytopathic effects was noted on the plates. Utilizing techniques outlined by Reed and Muench, TCID50 was calculated (8).

1.3.9 Cytopathic Effect (CPE) reduction

A poly-L-lysine pre-coated 24-well cell culture dish was used to seed HEK-ACE2 cells, which were then used for infection 24 hours later. The cells were pretreated with 1 μM Auranofin for three hours in triplicates. After that, they were incubated for one hour at 37°C with 0.1 MOI SARS CoV-2 in 100 μL of inoculum. The cells were then given 400 μL of complete media that contained the same amount of drug as before. Using the dye exclusion method of Trypan blue, the percentage of viable cells was determined after 48 hours.

1.3.10 Animal experiment

Animal handling: Male and female Syrian golden hamsters, aged 10 to 12 weeks, were used in all animal studies. They were acquired from Biogen Laboratory Animal Facility in Karnataka, India. The animals were provided with unlimited access to water and pellet meals during their three days of acclimatization at the experimental site. Males and females were housed apart in the Viral Biosafety level-3 facility at the Indian Institute of Science, with a 12-hour day/night light cycle. A combination of ketamine (Bharat Parenterals Limited) and xylazine (21, Indian Immunologicals Ltd.) overdose was used to euthanize the hamsters.

Toxicity and virus challenge: On Syrian golden hamsters, the toxicity of 1 and 5 mg/kg bodyweight Auranofin was evaluated through oral administration of the drug once daily in 200 μl PBS. The conversions described in https://www.fda.gov/media/72309/download correspond to a dosage of 1 mg/kg (Hamster) x 0.13 (conversion factor) = 0.13 mg/kg (Human equivalent dose) and 5 mg/kg (Hamster) x 0.13 (conversion factor) = 0.65 mg/kg (Human equivalent dose) of auranofin per day. The hamsters' total body weight was monitored for a total of seven days. In order to conduct infection tests, animals were intranasally inoculated with 10^5 PFU of SARS-CoV-2 in 100 μL of PBS. Before infection, the animals were anesthetized using intraperitoneal injections of a mixture of ketamine (150 mg/kg) and xylazine (10 mg/kg). The prophylactic

regimen involves administering Auranofin (5 mg/kg/day) orally 3, 3, and 1 day prior to infection and then being challenged with the virus on day zero. Auranofin (5 mg/kg/day) was administered orally as part of the therapeutic treatment regimen beginning 24 hours after infection (hpi) and continuing for two and three days after infection (dpi). Throughout the trial, daily records of the total body weight were made, and at 4 dpi, the animals were sacrificed. By using qRT-PCR, the viral RNA load in lung tissue specimens was determined. Based on earlier research, the sample size for hamster experiments was determined (9, 10).

1.3.11 RT PCR for viral RNA

Total RNA was isolated for qRT-PCR using TRIzol™ Reagent in accordance with the manufacturer's instructions. Equal amounts of RNA were used to determine viral load using AgPath-ID^{TM} One-Step RT-PCR kit (AM1005, Applied Biosystems). Using the SARS-CoV-2 genomic RNA standard, a standard curve was generated to determine the viral RNA copy number using primers and probes targeting the SARS CoV-2 N-1 gene (Forward primer: 5′GACCCCAAAATCAGCGAAAT3′ and Reverse primer: 5′ TCTGGTTACTGCCAGTTGAATCTG3′, Probe: (6-FAM / BHQ-1) ACCCCGCATTACGTTTGGTGGACC).

1.3.12 Quantitative RT PCR for host mRNA

Using the Prime ScriptTM RT Reagent Kit with gDNA Eraser (Perfect Real Time) (RR047A, Takara-Bio), equal amounts of RNA were converted into cDNA. The cDNA was then diluted with 80µl nuclease-free water. PowerUpTM SYBRTM Green Master Mix (A25778, Applied BiosystemsTM) was used for the gene expression analysis, along with the proper primers for each gene and 18srRNA as the internal control.

1.3.13 Histopathology

Hamster lung tissue samples were embedded in paraffin blocks after being treated in 4% paraformaldehyde in PBS. Hematoxylin and Eosin (H&E) was used to stain tissue sections with a thickness of 4-6 µm for light microscopy analysis, as previously reported (11).

1.3.14 NFκB reporter assay

Pre-coated 24-well plates were used to seed HEK 293T cells. After a day, 500 ng of empty vector, 20 ng of pRL-TK, and 50 ng of NFκB-promoter driven firefly luciferase plasmid were co-transfected into the cells using lipofectamine 2000. After twenty-four hours, the cells were

pre-treated with 1μM auranofin for three hours, and then TNFα was induced while the drug was present. After 12 hours, cells were lysed and the INFINITE M PLEX Tecan plate reader was used to measure the amount of luciferase activity.

1.3.15 Entry assay

A poly-L-lysine pre-coated 96-well cell culture dish was used to seed HEK-ACE2 cells, which were then used for infection 24 hours later. The T-3 experiment involved pre-treating cells with 1μM Auranofin for three hours, followed by SARS-CoV-2 viral infection at 10 MOI for three hours. In the T+6 assay, cells were infected with the SARS-CoV-2 virus at a multiplicity of infection (MOI) of 10. After 6 hours, 1μM Auranofin was added, and the cells were incubated for 3 hours. The cells were collected for RT PCR (harvested in TRIzol) and western blot (lysed in 1X Laemmli buffer).

1.3.16 FlipGFP^{Mpro} assay

HEK 293T cells were transfected with 125 ng of Mpro reporter plasmid and 375 ng of NSP5 WT plasmid using lipofectamine 2000 in order to examine the impact of auranofin. Three hours later, fresh DMEM containing 1 μM auranofin was added to the media. After 36 hours cells were fixed with 4% formaldehyde and imaged using Evos M5000 microscope.

1.3.17 IC90 calculation

24-well plates coated with poly-L-lysine were used to seed HEK ACE2 cells. After 24 hours, the cells were pre-treated with molnupiravir (20, 10, 5, 2.5 and 1.25 μM), nirmatrelvir (100, 80, 75, 60, 50, 25, 16, 10 nM), and remdesivir (1 μM, 0.5 μM, 0.25 μM, 125 nM, 100 nM, 60 nM, 20 nM, 16 nM, and 4 nM) for three hours. Finally, the cells were infected with luciferase-expressing SARS-CoV-2 virus at 0.1 MOI. The luciferase activity of the cells was tested 48 hours later. The percentage of infection was adjusted to the infected control, and GraphPad Prism v8.0.2 or Excel was used to calculate IC90.

1.3.15 Drug combination

After seeding HEK ACE2 cells in 24-well plates coated with poly-L-lysine, the cells were treated with IC90, IC45, or IC22.5 of molnupiravir, nirmatrelvir, or remdesivir for three hours, and then infected at 0.1 MOI with a luciferase-expressing SARS-CoV-2 virus. The luciferase activity of the cells was tested 48 hours later. Infection percentage was compared to the infected control.

1.4 Results

1.4.1 Compilation and overlap analysis of published transcriptomics and proteomics data

We began our study with the aim to identify host-factors that are upregulated at the upper respiratory tract, the primary site of SARS-CoV-2 infection. For this, we have utilised a 'top-down' approach. We selected 4 transcriptome (T) and 3 proteome (P) datasets (7), where samples were collected from the nasal swabs and bronchoalveolar lavage fluid (BALF) with healthy individual as control (Figure 1A). We performed meta-analysis using applied a rationally designed workflow (Figure 1B). Briefly, a) 1.5 fold upregulation at mRNA and protein levels with p value (≤0.01) or q value (≤0.05) were kept as cut-off for shortlisting. The data was filtered so that only significantly upregulated genes from each sample were sorted. b) The filtered genes and/or proteins from each study were subjected to a pairwise overlap analysis, and genes that significantly overlapped were identified. c) Cumulative scores of the upregulated genes were computed by summing the log2 fold change values in their respective parent datasets and then ranked, d) Genetic markers that were selected were experimentally validated to determine their prognostic and therapeutic significance. Here, in this project I will discuss about exploring the therapeutic potential of the upregulated host factor.

A

Study Type	Study ID	Tissue type	Description	Reference
Transcriptomics	T1	Nasopharyngeal Swabs	Patients 430, Healthy Controls 54	Liberman et al.
	T2	BALF	Patients 86, Healthy Controls 5	Grant et al.
	T3	BALF	Patients 2, Healthy Controls 3	Xiong et al.
	T4	BALF	Patients 8, Healthy Controls 20	Zhou et al.
Proteomics	P1	Nasopharyngeal Swabs	5 positive and five negatives oro- and nasopharyngeal swabs	Rivera at al.
	P2	Nasopharyngeal and oropharyngeal swabs	15 PCR Positive and 15 PCR Negative Patients	Akgun et al.
	P3	Nasopharyngeal and oropharyngeal swabs	20 Positive and 20 Negative Patients	Maras et al.

B

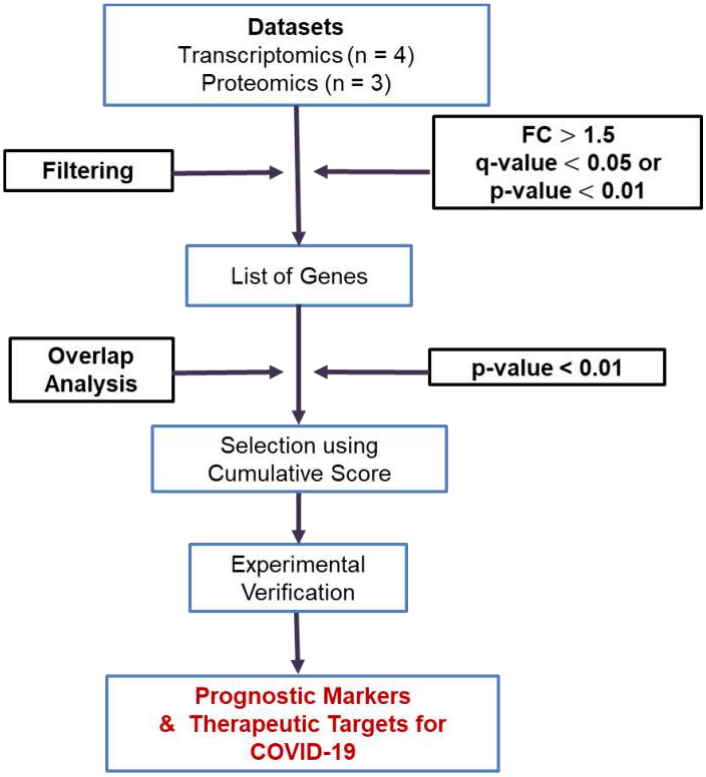

Figure 1: Workflow of Meta-analysis for shortlisting upregulated host-factors. A) List of transcriptome and proteome datasets. B) Meta-analysis pipeline.

1.4.2. Thioredoxin: a candidate for host-directed therapy

During the meta-analysis, an orthogonal pair-wise overlap analysis was performed between transcriptome and proteomes datasets, T1-T3 (14), T1-T4 (9), T1-P3 (2), T3-T4 (504), T3-P1 (10), T3-P2 (8), T3-P3 (17), T4-P1 (8). T4-P3 (15) and P1-P3 (3) (Figure 2A). Here, using Fisher's exact test, a statistical analysis was performed (p-value < 0.01) between the transcriptome and proteome datasets. This method was adapted from a published literature (12)

where similar overlap analysis was performed to compare virus-host interaction and identify the significant overlap. From here, 566 significantly upregulated genes were identified and a Venn diagram was generated using the genes derived from significant intersections between proteomic or transcriptome datasets by pairwise overlap analysis. We observed that, at the end of the analysis, there is one gene that passed the rigor of meta-analysis, and appeared at the centre of TT-TP-PP datasets. This gene is thioredoxin (TXN) (Figure 2B). next, we explored the potential of TXN as therapeutic candidate.

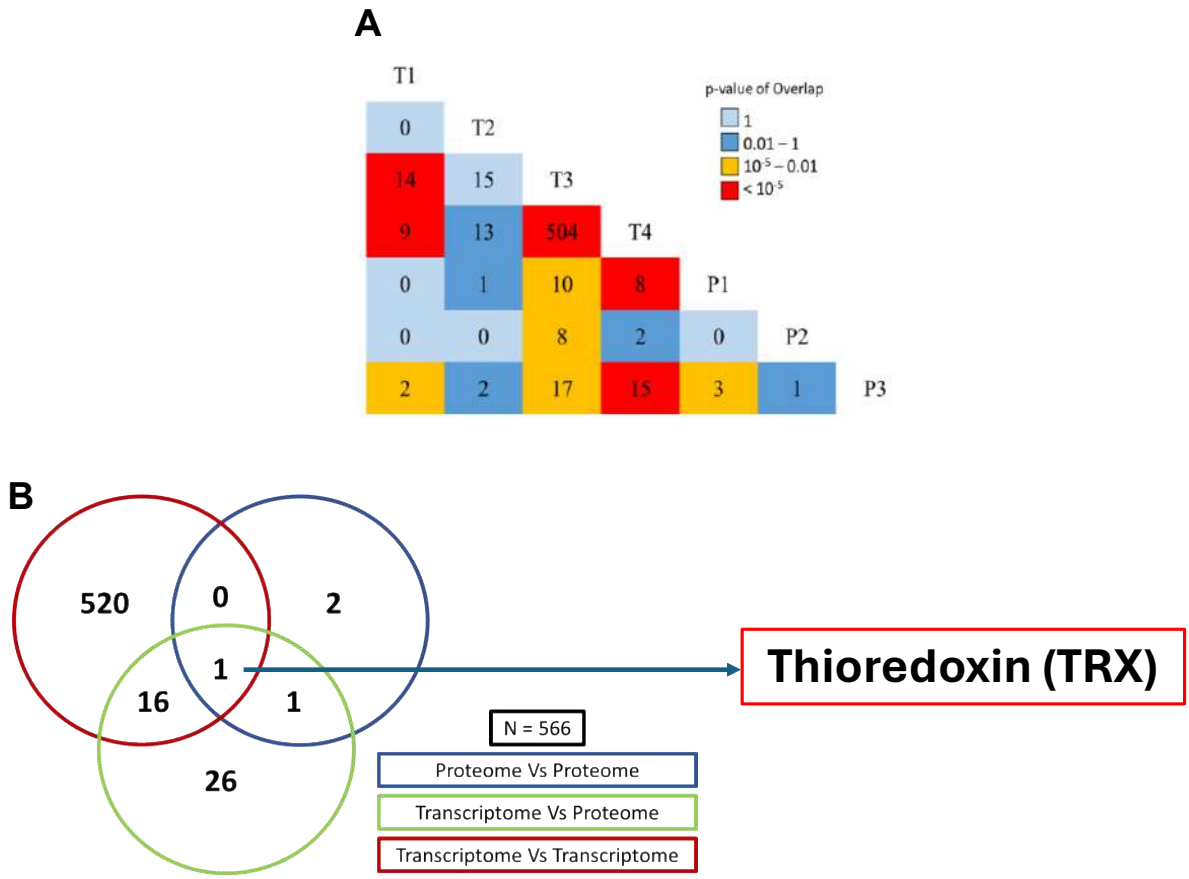

Figure 2: Thioredoxin is significantly upregulated at the URT. A) Heat-map showing the significant intersection of transcriptome and proteome datasets. Here, significance is denoted by the colour of the box. B) Venn diagram of genes derived from significant intersections between T and P datasets.

1.4.3 Testing the efficacy of Auranofin: *in vitro*

Thioredoxin is known for its ability to promote the production of inflammatory cytokines, induce apoptosis, and control redox status. It achieves this by transitioning between oxidized and reduced forms through the facilitation of thioredoxin reductase activity (13-15). Thioredoxin reductase has an FDA-approved inhibitor, called Auranofin, 2,3,4,6-tetra-o-

acetyl-L-thio-β-D-glycopyranp-sato-S-(triethyl-phosphine)-gold (16). So, we evaluated the antiviral effectivity of Auranofin against SARS-CoV-2 infection. We began our exploration by performing cytotoxicity of Auranofin in HEK ACE2, where 1, 2, and 4 μM dose was tested. We found that 1 μM is well-tolerated (Figure 3A), thus we proceeded with antiviral assay at 1 μM concentration. HEK ACE2 cells were pre-treated with 1 μM Auranofin for 3 hours, and then cells were infected SARS-CoV-2 at 0.1 MOI for 48 hours (Figure 3B). We observed that Auranofin treatment has reduced virus infection associated cytopathic effect (CPE) and rescued cell viability up to 6-fold (Figure 3C, D). Next, we tested the increasing dose of Auranofin in HEK ACE2 and measured the effect on viral RNA (vRNA) level. We observed that after 1 μM Auranofin treatment, vRNA is reduced almost 3 logs. We determined the IC_{50} as 0.29 μM (Figure 3E). We also checked the effect at viral protein, which also corroborated the RT PCR result. We observed that spike protein was completely absent after 1 μM Auranofin treatment (Figure 3F). Furthermore, infectious viral titer by plaque assay showed reduction in virus infection after Auranofin treatment. Taken together, these suggest that Auranofin treatment mitigated virus infection *in vitro*.

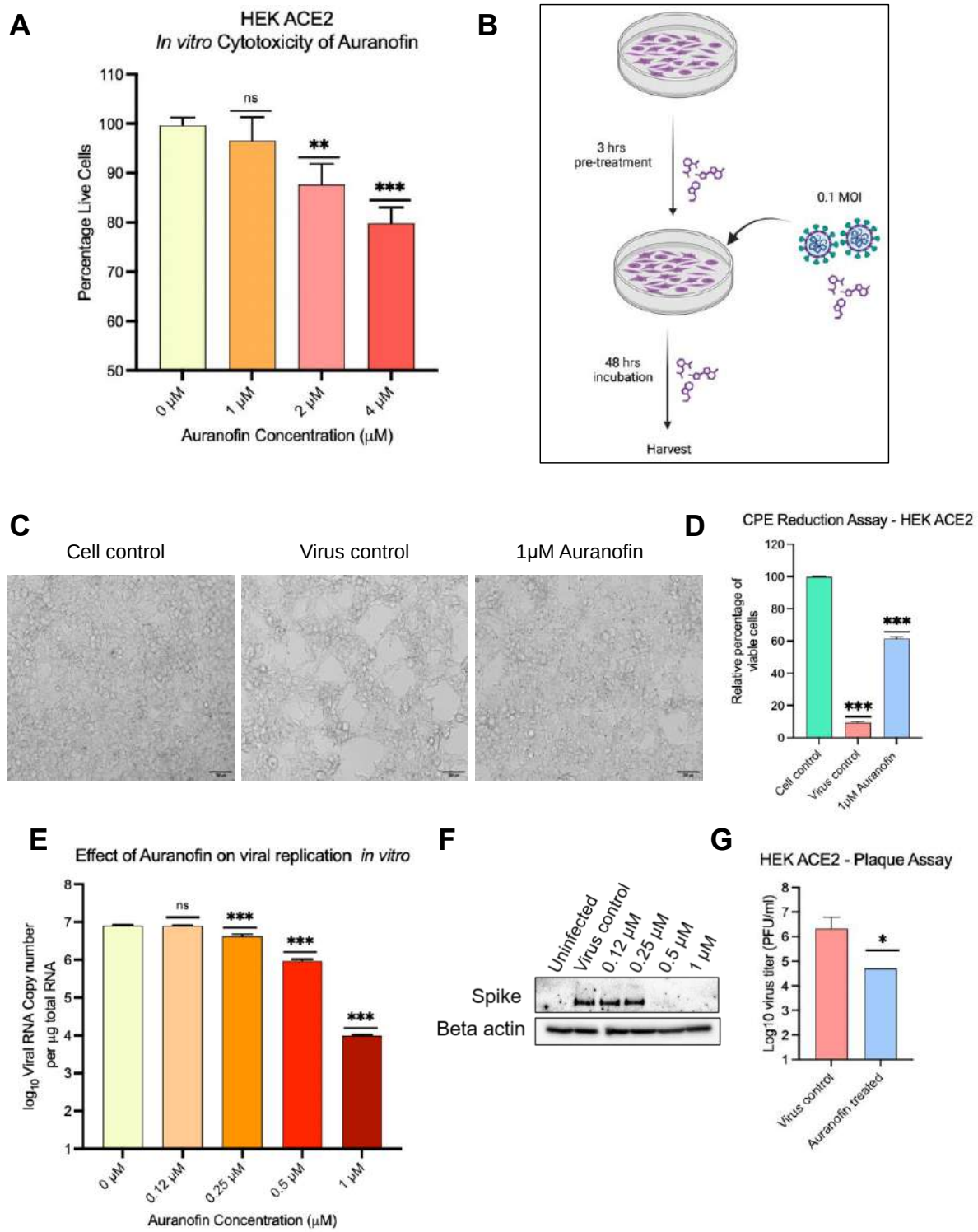

Figure 3: Auranofin inhibits SARS-CoV-2 infection in HEK ACE2 cells. A) Cytotoxicity of Auranofin in HEK ACE2 cells. B) Schematic representation of antiviral assay of Auranofin in HEK ACE2 cells. C) Representative microscopic images cytopathic effect after SARS-CoV-2 infection. D) Quantification of CPE. Live cells were quantified using trypan blue. E) Log_{10} vRNA quantification using RT PCR. F) Western blot images of SARS-CoV-2 spike protein

after Auranofin treatment at indicated doses. G) Plaque assay analysis of infectious virus titer after Auranofin treatment.

Additionally, we validated the antiviral effect of Auranofin in another cell line. For that, we have used Vero E6. Just like previously done, we began by performing cytotoxicity assay in Vero E6 at 1, 2, and 4 µM Auranofin. We observed minimal toxicity at 1µM Auranofin (Figure 4A) and proceeded with antiviral assay. Vero E6 cells were pre-treated with 1µM Auranofin for 3 hours, and then infected with SARS-CoV-2 virus at 0.001 MOI for 48 hours (Figure 4B). Viral RNA quantification using RT PCR revealed reduction in infection after Auranofin treatment (Figure 4B). Plaque assay also reflected the same (Figure 4C). Collectively, Auranofin mitigates SARS-CoV-2 infection cell culture.

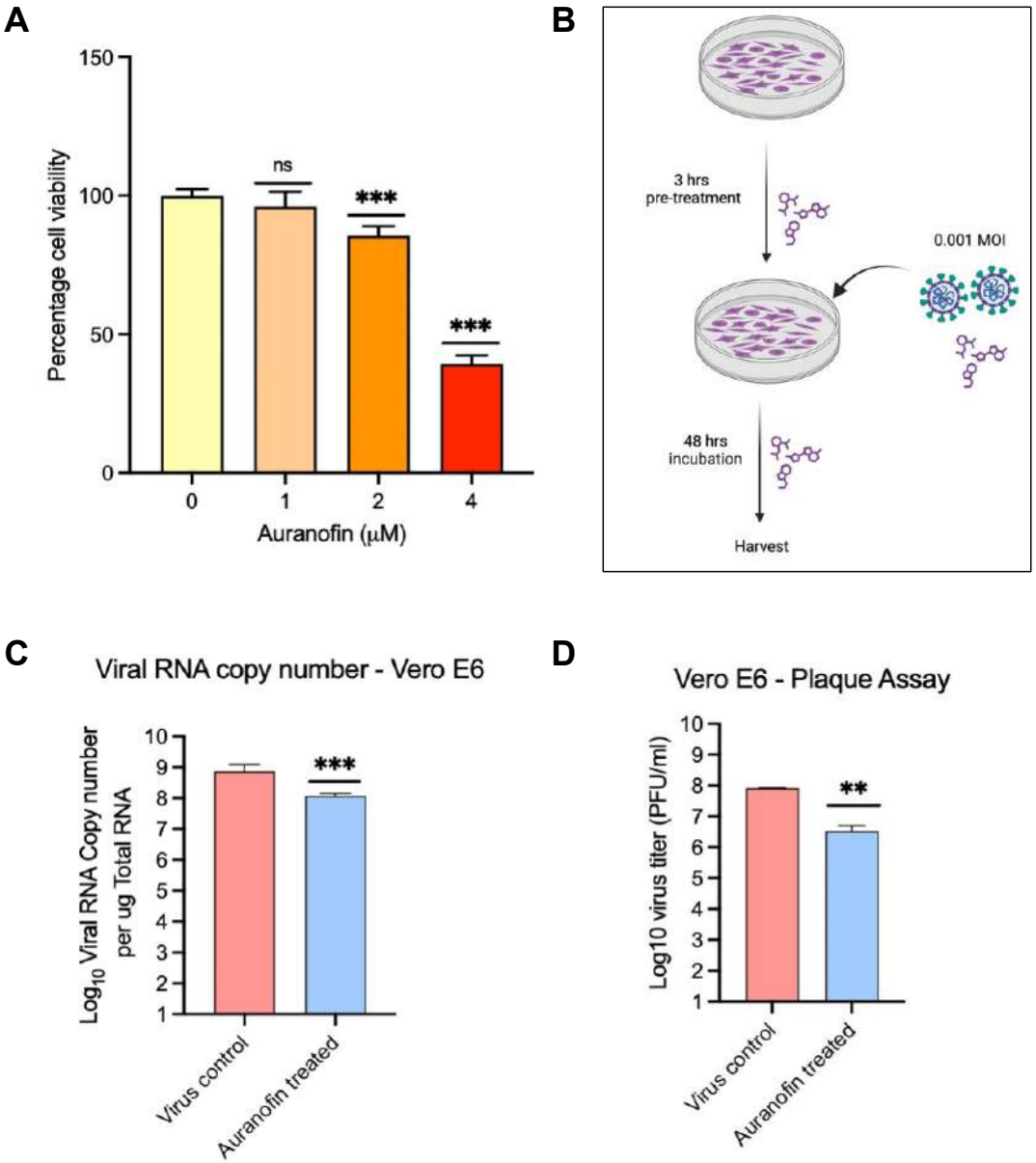

Figure 4: Auranofin inhibits SARS-CoV-2 infection in Vero E6 cells. A) Cytotoxicity of Auranofin in Vero E6 cells. Cell viability was quantified using Alamar blue reagent. B) Schematic representation of Antiviral assay in Vero E6 cells. C) Log_{10} vRNA quantification using RT PCR. D) Plaque assay of cell culture supernatant after Auranofin treatment.

1.4.4 Testing the efficacy of Auranofin: *in vivo*

Next, we validated the antiviral effect in animal model. For that, we used Syrian golden hamster, a preferred animal model of choice for testing vaccines and antivirals against SARS-CoV-2 (11). We started by performing the toxicity of Auranofin in hamsters, where drugs were administered once daily via oral route at 1 mg/kg body weight or 5 mg/kg body weight. We observed that animals continued to gain at both of the tested doses, suggesting that both of the doses are well-tolerated (Figure 5A). So, we proceeded with animal challenge at 5 mg/kg body weight. For infection studies, he drug was administered orally in two formats, prophylactic and therapeutic: before infection and after infection, respectively (Figure 5B). When compared to the vehicle control group, the viral titers in the hamster lungs at Day 4 showed that both prophylactic and therapeutic administration of Auranofin at a non-toxic dose of 5 mg/kg body weight was more effective at mitigating virus replication in lung tissue (Figure 5C). Auranofin treatment also rescued the body weight loss due to infection compared to vehicle control infected group (Figure 5D). Examining the histological sections of lungs stained with Hematoxylin and Eosin revealed clear evidence of cellular infiltration and damage to the alveolar epithelial lining in infected animal lungs (Figure 5E, top right, yellow circle 2). Auranofin treatment have reduced this lung inflammation, both in prophylactic and therapeutic (Figure 5E, bottom panels, yellow circle 3 & 4). Moreover, TXN has been shown to increase the production of proinflammatory cytokines, particularly IL-6, a known modulator of the severity of COVID-19 (17, 18). Thus, we have checked the effect of Auranofin treatment on IL-6 production in the infected lungs and found it to be significantly reduced (Figure 5F). these data suggests that Auranofin treatment mitigates SARS-CoV-2 infection *in vivo*.

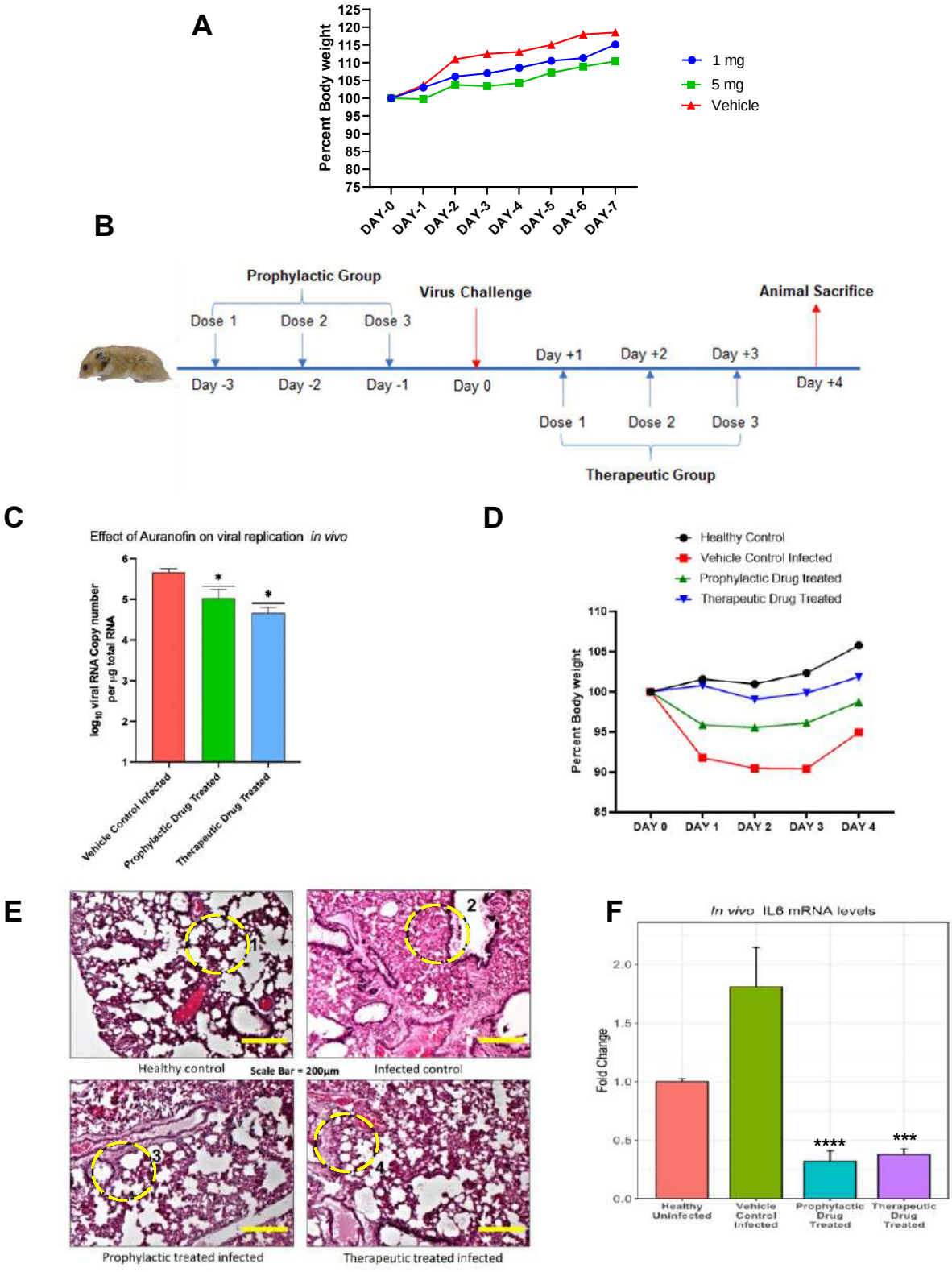

Figure 5: Auranofin mitigates SARS-CoV-2 infection in Syrian golden hamster. A) Toxicity of Auranofin in Syrian golden hamster. B) Timeline of animal experiments involving 10-12 week old hamsters (n=4). C) Viral RNA quantification from the infected lungs. D) Body weight measured from D0 to D4, considering weight on D0 as 100% (n=4). E) H & E staining

of hamster lungs, showing healthy control, infected control, prophylactic and therapeutic. The areas marked in the circle show following (1) Normal healthy alveolar lining and morphology (2) Alveolar damage, cellular infiltration, inflammation (3,4) Protected alveolar morphology and reduced infiltration, inflammation. (scale bar - 200µm). F) IL-6 mRNA levels were measured from the total RNA isolated from hamster lungs.

1.4.5 Mechanism of action of Auranofin

So far, we have seen that Auranofin inhibits SARS-CoV-2 infection *in vitro* and *in vivo*, probably by inhibiting inflammatory IL-6 cytokine production. Next, we wanted to elucidate the mechanism of action. So began by testing the effect on the NFκB pathway, one of the most important inflammatory pathways. HEK 293T cells are co-transfected with Firefly luciferase reporter plasmid where luciferous gene is cloned downstream of NFκB promoter, constitutively renilla luciferase expressing pRLtK plasmid which is an internal control and an empty vector. 24 hour post transfection, cells were pre-treated with drug for 3 hours followed by induction with TNFa and 12 hours later Luciferase activity is measured (Figure 6A). We observed ~30% reduction in NFκB promoter activity after auranofin treatment (Figure 6B).

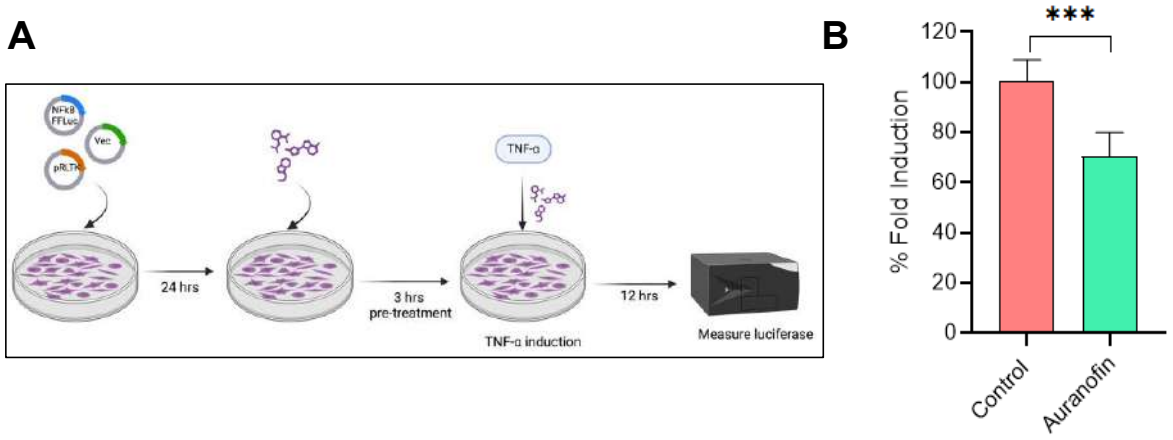

Figure 6: Effect of Auranofin on NFκB promoter activation. A) Schematic representation of the experiment outline. B) % fold induction of NFκB promoter activation in presence and absence of Auranofin.

Next, we wanted to test whether Auranofin has any direct effect on different stages virus lifecycle. We began by testing the effect at entry, for which we used a non-replicating luciferase expressing SARS-CoV-2 spike pseudotyped virus (19). To test the effect of auranofin on pseudotype virus entry, HEK

ACE2 cells were pre-treated with Auranofin for 3 hours, followed by infection with pseudo type virus in presence of the drug and 48 hours later luciferous activity are measured (Figure 7A). Here we found reduced luciferase units in presence of Auranofin treatment (Figure 7B), suggesting that it has inhibited the entry of pseudotype virus. Moving forward, we wanted to check whether auranofin treatment can inhibit entry of SARS CoV-2. For that we have performed time of addition experiment (ToA). Here, HEK ACE2 cells were infected with SCoV2 virus and harvested after 3 hours (virus control or VC) or cells were pre-treated with the drug for 3 hours, followed by infection in presence of the drug for another 3 hours (T-3) (Figure 7C). We observed a reduction at viral spike protein band intensity after auranofin treatment, suggesting Auranofin reduces virus entry (Figure 7D & E). To further potentiates our claim, we performed another ToA experiment, where drug was administered 6 hours post infection, and virus protein and intracellular viral RNA levels were measured (Figure 7F). we observed that drug administration at later stages of virus infection has no effect on viral protein level (Figure 7G & H). Furthermore, there was no impact on intracellular vRNA level (Figure 7I), suggesting that Auranofin inhibit virus entry and also, it does not affect the viral polymerase activity.

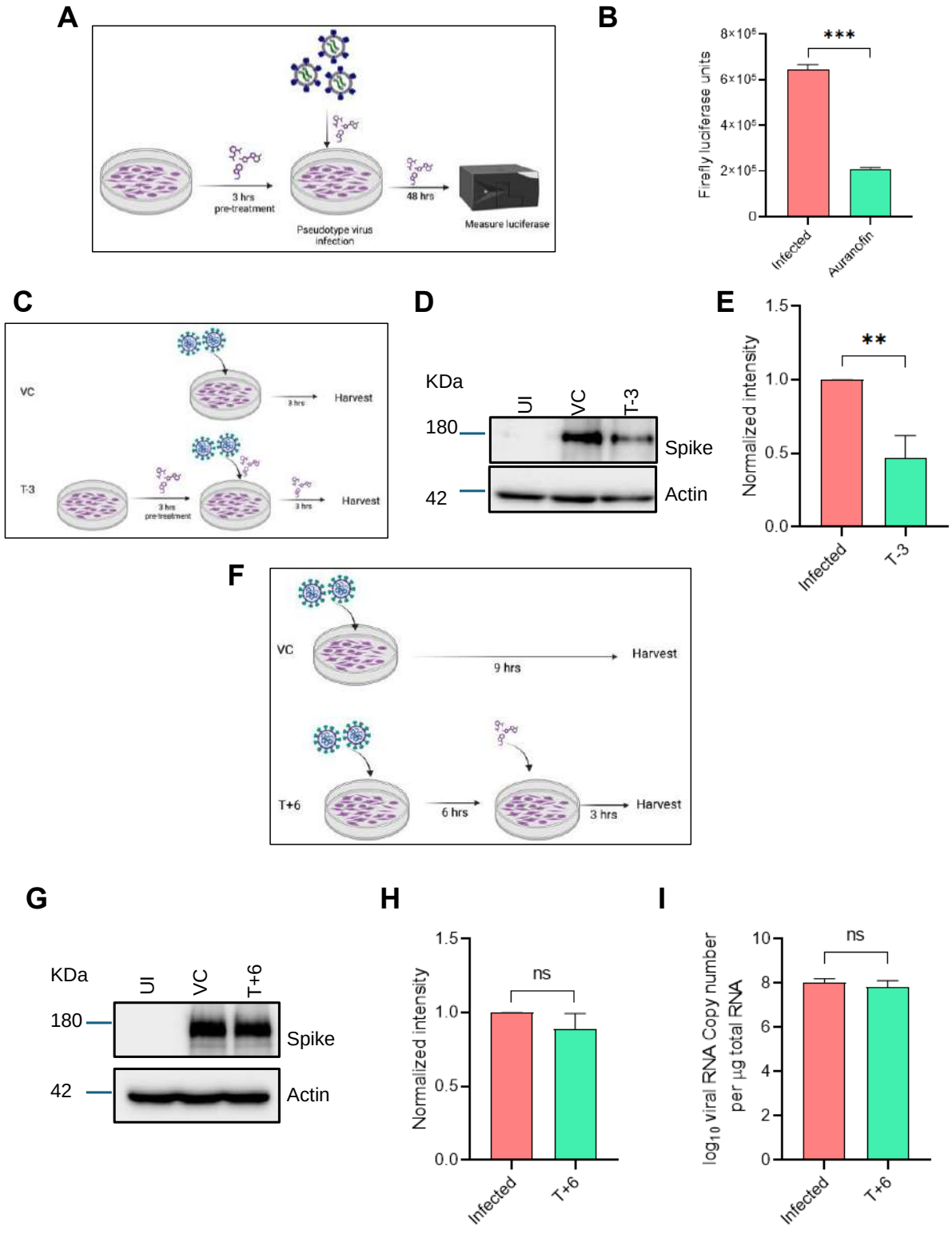

Figure 7: Effect of Auranofin on virus entry. A) Schematic representation of pseudotype virus entry assay. B) Effect of Auranofin on pseudotype virus entry shown as luciferase units. C) Schematic representation of ToA assay. D) SCoV2 spike protein level in absence of Auranofin (VC) and in presence of Auranofin (T-3). E) Quantification of spike band intensity from Figure panel D. F) Schematic representation of ToA assay where drug is administered 6

hpi. G) SCoV2 spike protein level in absence of Auranofin (VC) and in presence of Auranofin (T+6). H) Quantification of spike band intensity from Figure panel G. I) Intracellular viral RNA levels measured from HEK ACE2 cells. Experiment outline is depicted in panel F.

After virus entry, viral RNA is released into the cytoplasm, which is subjected to immediate translation and polyprotein processing mediated by papain-like protease and main protease (Mpro, encoded by NSP5) (20). So next we tested the effect on main protease activity using a FlipGFP-M^{pro} reporter construct, where GFP 1-9 and GFP10-11 is separated using a coiled-coil domain and kept it in parallel orientation, i.e., flipped orientation. Cleavage of the linker sequence by Mpro restores the GFP structure and reconstitute GFP expression and it has mCherry as internal control (21). Next, we used this reporter and tested the effect of auranofin on the main protease activity. HEK 293T cells are transfected with nsp5 WT, main protease reporter. 3 hours post-transfection, media was replaced with fresh DMEM containing Auranofin and 24 hours later cells were fixed to measure the GFP intensity (Figure 8A). Here we have tested auranofin, and nirmatrelvir, which is a known inhibitor of nsp5. We observed a reduction in GFP intensity in presence of Auranofin, similar to Nirmtarelvir (Figure 8B & C). these data suggest that auranofin can inhibit main protease activity.

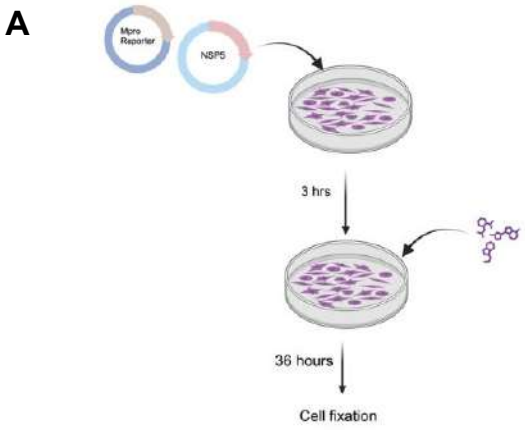

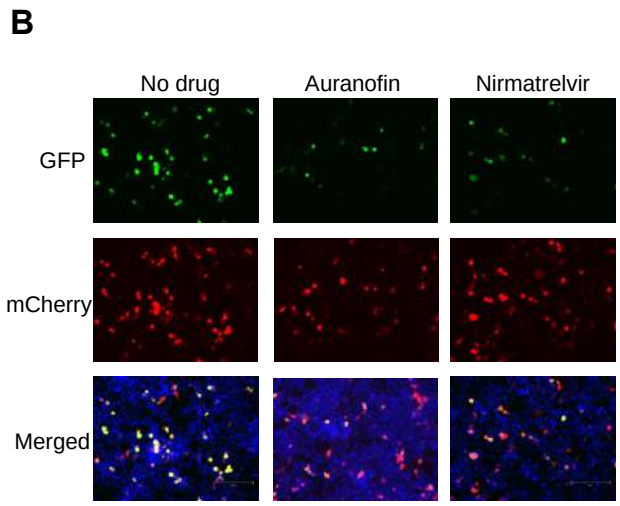

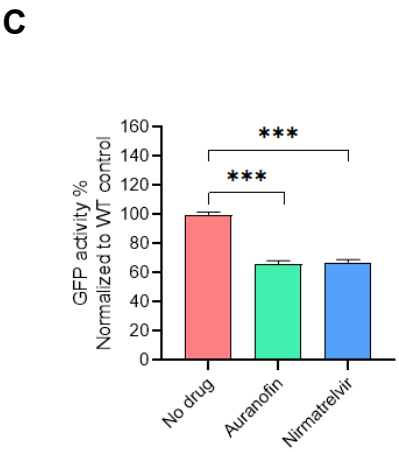

Figure 8: Effect of Auranofin on Mpro activity. A) Schematic representation of FlipGFP-M^{pro} reporter assay in presence of Auranofin. B) Representative images of GFP, mCherry channel. C) Quantification of the GFP intensity.

1.4.6 Auranofin in combination with nucleoside analogues

Both in vitro and in vivo, auranofin demonstrated potent antiviral efficacy against SARS-CoV-2. Subsequently, we aimed to evaluate auranofin in combination therapy with direct-acting antivirals or DAAs. In this context, we evaluated the synergy with nucleoside analogues, like remdesivir and molnupiravir and Mpro inhibitor like nirmatrelvir. We began by determining the IC_{90} of the drugs (Figure 9A-D), using a nanoluciferase expressing SARS-CoV-2 reporter virus (22). Next, we proceeded with the combination testing, where IC_{90}, IC_{45}, and $IC_{22.5}$ of the DAAs were tested in combination with IC90 and IC45 of Auranofin. We observed a synergistic effect of Auranofin with remdesivir and molnupiravir, where former showed better synergy (Figure 9 E & F). Here, IC45 of combination of two drugs (Auranofin with remdesivir or molnupiravir) showed reduced virus infection compared to individual drugs (Figure 9E & F). However, combination of Auranofin with nirmatrelvir did not enhance the protective effect against SARS-CoV-2 infection (Figure 9G), probably associated with competitive effect on Mpro activity. These data suggest that HDT candidate Auranofin in combination with DAAs, remdesivir and molnupiravir showed enhance protection against SARS-CoV-2 infection.

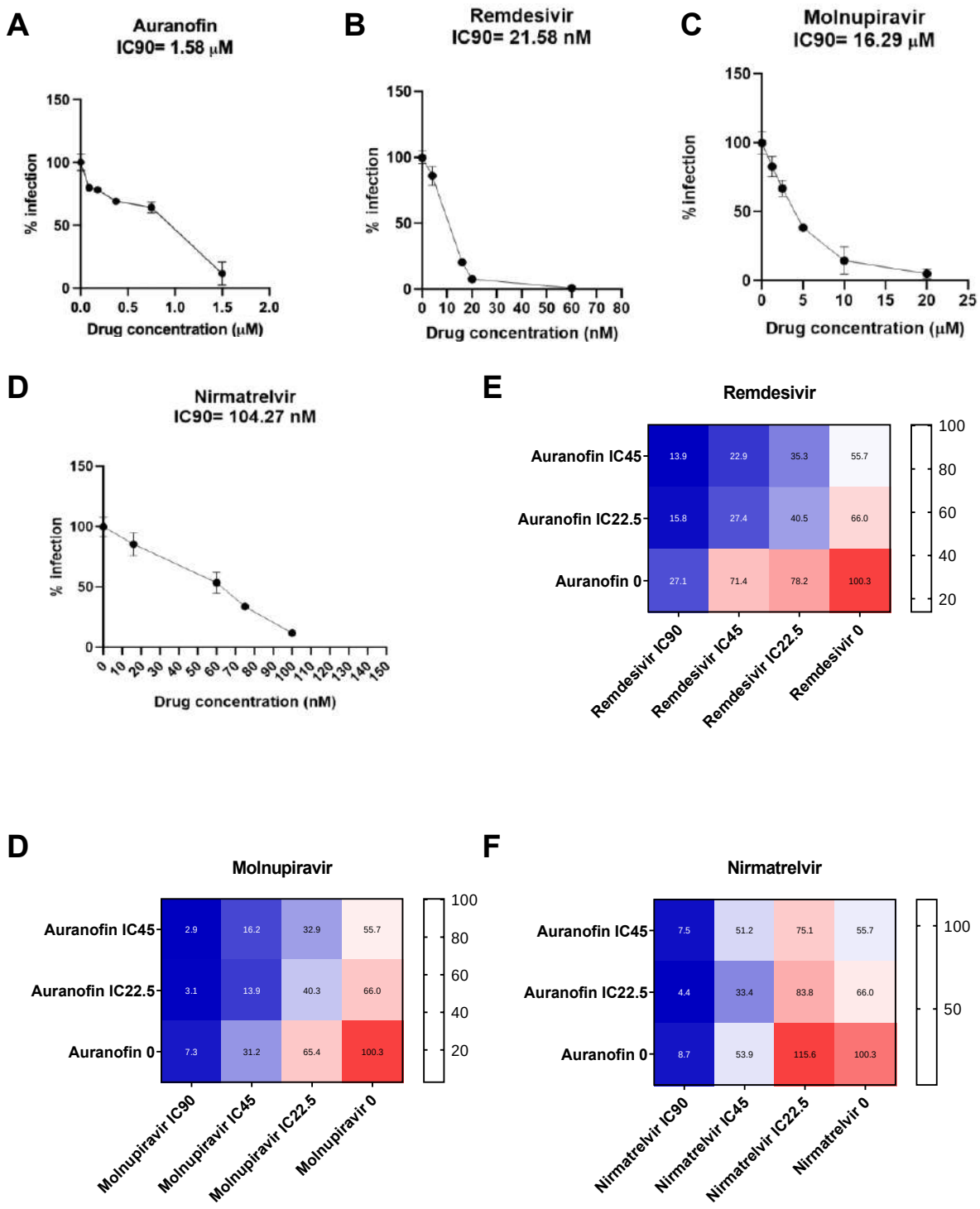

Figure 9: Auranofin in combination with direct-acting antivirals. A-D) IC90 determination using a luciferase expressing SARS-CoV-2 reporter virus of Auranofin (A), Remdesivir (B), Molnupiravir (C), and Niramterlvir (D). E-F) Combination of IC_{90}, IC_{45}, and $IC_{22.5}$ of remdesivir (E), molnupiravir (F), and nirmatrelvir (F) with IC_{45}, and $IC_{22.5}$ of Auranofin.

1.5 Statistical Analysis

Statistical analyses and overlaps were performed in the R statistical environment version 4.0.3 via RStudio version 1.3.1093. All numerical data of bar graph were analyzed and plotted using GraphPad Prism v8.0.2. Statistical significance was calculated using a *t* test with Bonferroni corrections for multiple comparisons (wherever necessary). The P values were indicated as $*P < 0.05$; $**P < 0.01$; $***P < 0.001$; ns = not significant. Error bars represent mean + standard error.

1.6 Discussion

In order to identify high-confidence upregulated host components, we performed a meta-analysis of published transcriptome and proteome profiles of respiratory samples of COVID-19 patients. Guided by this analysis, we found that thioredoxin (TXN) was found to be consistently upregulated. We demonstrated that Auranofin, which inhibits thioredoxin reductase, reduces SARS-CoV-2 replication in vitro. Moreover, oral auranofin administration as part of a therapeutic and prophylactic regimen decreased lung inflammation, IL-6 production, and viral replication in Syrian hamsters. Furthermore, we explored the mechanism of action of Auranofin and showed that it inhibits inflammatory NFκB pathway, virus entry and viral main protease activity. In addition, we showed that Auranofin works synergistically with Remdesivir and Molnupiravir and enhance antiviral activity against SARS-CoV-2.

1.7 Impact of the research in the advancement of knowledge or benefit to mankind

At the early days of pandemic, several researchers profiled host response at the upper respiratory tract, the primary site of infection. While these Big data holds the key to therapeutic strategies, translation of these knowledges into antiviral strategies were lacking. Thus we have employed meta-analysis using these published OMICS datasets and identified thioredoxin as most consistently upregulated host factor. We showed that Auranofin, which is an FDA-approved inhibitor of thioredoxin reductase, has antiviral activity against SARS-CoV-2. Auranofin is an orphan drug which is used for the treatment of rheumatoid arthritis. In our study, we demonstrated that Auranofin mitigates SARS-CoV-2 infection in cell culture as well as in Syrian golden hamster. Additionally, we are among the pioneers in India to establish cell culture and animal models for studying SARS-CoV-2 under the challenging conditions of the COVID-19 pandemic. Our study emphasizes the importance of meta-analysis, how it can help in identifying potential therapeutic candidate from OMICS datasets. Furthermore, we show the importance of drug repurposing during this pandemic situation.

Potent direct acting antivirals like remdesivir, molnupiravir comes with certain drawback, such as teratogenic activity, appearance of resistance. Thus a combination of DAAs with host-

directed therapeutics targeting different steps of life cycle will potentiate the antiviral activity. Here our study demonstrate that combination therapy of Auranofin with remdesivir and molnupiravir works in synergistic manner. This will help to reduce the required amount of remdesivir and molnupiravir, thus reduce the teratogenicity and increase the resistance barrier. Moreover, our study sheds new light on the importance of meta-analysis in identifying new antivirals, antiviral activity of Auranofin against SARS-CoV-2 infection for combination therapy.

II) To characterize cellular antiviral response against SARS-CoV-2 and viral evasion and antagonism strategies.

2.1 Introduction

One of the earliest antiviral responses is orchestrated by interferon (IFN), which poses a crucial barrier that virus needs to overcome to establish infection. Innate immune pathway consists of two parts: IFN induction and IFN signalling pathway. IFN response begins with recognizing viral RNA by sensors like RIG-I and MDA5. These proteins activate a cascade of signalling pathway, beginning with RIG-I activation. Activated RIG-I interacts with MAVS and stimulate two kinases, TBK1 and IKKe. These kinases in turn auto phosphorylate and mediates IRF3 phosphorylation. IRF3 phosphorylation prompts its dimerization and facilitate nuclear translocation where it binds to the IFNβ promoter and activate transcription of IFNs. These IFNs are secretory molecules, act in autocrine and paracrine manner. It binds to the IFN alpha receptors (IFNAR) and activate Janus Kinase 1 (JAK1) and tyrosine kinase 2 (TYK2). They mediate phosphorylation of signal transducer and activator of transcription (STAT) 1 & 2. Phosphorylated STAT1 and STAT2 binds with IRF9 and translocate to nucleus where it binds to the ISG promoter (called interferon stimulated response element or ISRE) and stimulate interferon stimulated genes (ISGs) transcription (Figure a) (23).

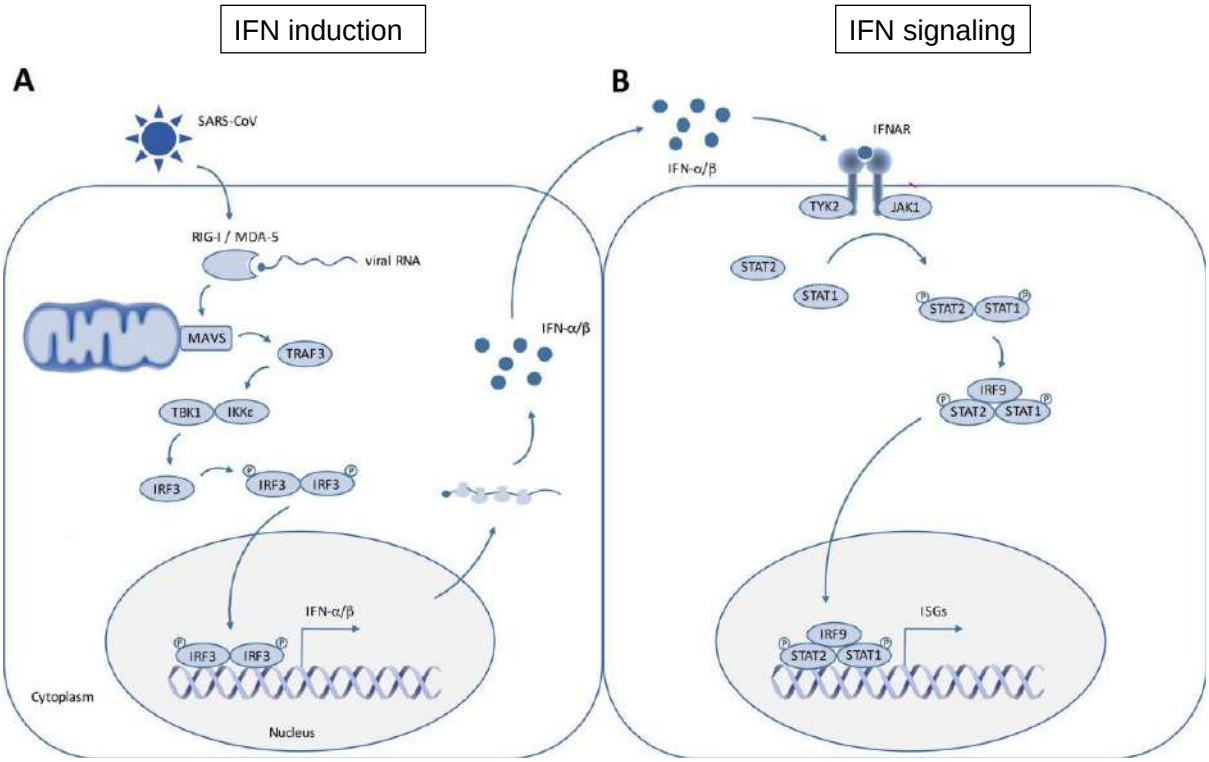

Figure a. Schematic of innate immune pathway. It consists of two parts: IFN induction and signalling pathway. Viral RNA cues recognition by host pattern recognition receptors (PRRs) like RIG-I or MDA5 activate downstream proteins that result in IFN production. This step is called as IFN induction pathway. Upon binding of IFNs with IFN alpha receptor (IFNAR), JAK1 and TYK2 is activated that in turn phosphorylate and activate STATs. Activated STATs bind to the ISG promoter and mediates the antiviral function. The schematic is adapted from (23).

SARS-CoV-2 is a single-stranded positive-sense RNA virus of the family *Coronaviridae* (24). Two overlapping open reading frames (ORFs) at 5′ end in the genome, ORF1a, and ORF1b, are translated into continuous polypeptides, which are proteolytically processed to produce 16 non-structural proteins (NSPs). Other one-third at the 3′ ends encodes multiple sub-genomic RNAs that get translated into structural proteins (spike, membrane, envelope, and nucleocapsid) and accessory proteins (ORF3a; 3b; 6; 7a; 7b; 8; 9b; 9c and 10) (25). Like other *betacoronaviruses*, SARS-CoV-2 encodes for an arsenal or proteins to antagonize the host immune pathway to establish a successful infection. Our aim is to identify the innate immune antagonists.

2.2 Objectives

Identify SARS-CoV-2 proteins that antagonize host innate immune pathway and elucidate the immune evasion mechanism.

2.3 Materials and Methods,

2.3.1 Plasmids and transfection

Professor Nevan Krogan of the University of California, San Francisco, generously provided us plasmids that express the SARS-CoV-2 proteins, which have been previously reported (26). Prof. Adolfo García-Sastre of the Icahn School of Medicine at Mount Sinai, New York, provided the IFN induction and signaling plasmids (IFNβ-Firefly Luciferase, ISRE-Firefly Luciferase, pRL-TK, RIG-I, 2-CARD, TBK1, IKKe, IRF3-5D, IRF7-CA, STAT1, STAT2) plasmids, which have been previously reported (27). ORF6 deletion and mutant variants were cloned in lab. Ubiquitin plasmids were procured from the Addgene. All the plasmids were transfected using lipofectamine 2000 according to manufacturer's instruction.

2.3.2 Dual-luciferase assay

HEK-293 T cells (0.1 X 106 cells/well in a 24-well plate) were co-transfected, in duplicate, with 500 ng of SARS-CoV-2 protein expression plasmid or empty vector in addition to 50 ng of pIFNβ -luc and 20 ng of pRL-TK for the IFN induction experiment. After 24 hours of transfection, cells were stimulated with either 100 HAU of the Sendai virus or poly (I:C) (1 μg) for a duration of 12 hours. Subsequently, the cells were lysed to assess the dual luciferase activity. In order to analyze the IFN induction pathway's steps, HEK-293T cells were co-transfected with 50 ng of inducer plasmid in addition to the plasmids mentioned above. After 24 hours, the cells were lysed. Similarly, for the IFN signaling assay, ISRE-luc Firefly Luciferase reporter plasmid was transfected, instead of IFN firefly luciferase plasmids, along with renilla reporter plasmid and SARS-CoV-2 plasmid. 24 hours later, cells were induced with 1000 U/ml of Universal Type-I IFN for 12 hours. Luciciferase activity was measured using Tecan plate reader (INFINITE M PLEX). The signals were represented as percentage fold change with respect to the induced vector.

2.3.3 Western Blot

The procedure is same as described on point 1.3.6. Here, additionally included primary antibodies, like anti-strep, anti-Flag, anti-HA, anti-V5, anti-NP, etc.

2.3.4 Immunoprecipitation

Following an ice-cold 1X PBS wash, 500 µl of Pierce lysis solution supplemented with phosphatase and protease inhibitor was used per 100 mm plate to lyse the transfected cells. The lysate was vigorously vortexed every ten minutes over a 30-minute ice incubation period. The samples were centrifuged at 13,000 rpm for 10 min at 4 °C after being sonicated twice at a 25% amplitude for 5 s ON and 5 s OFF. Either the cleared supernatant was kept at -80 °C or analyzed as whole cell lysate (WCL or Input) by immunoblotting. To perform immunoprecipitation, protein-G-coated magnetic beads were used to pre-clear lysates, and then specific antibodies were added to the cell lysates and incubated overnight. The complex was then pulled down by protein-G-coated magnetic beads (88847, Invitrogen). 1X Laemmli buffer was used directly for elution and then subjected to western blotting.

2.3.5 Immunofluorescence assay (IFA)

For all IFA studies, cells were seeded in a 24-well plate with coverslips. For IRF3 GFP nuclear translocation assessment, A549 cells were seeded and after 24 hours transfected with 500 ng of IRF3-GFP and 500 ng of SARS-CoV-2 protein-expressing plasmid using Lipofectamine-2000 reagent. 24 hours later cells were fixed. For, STAT1 GFP nuclear translocation assessment, Vero cells were seeded and after 24 hours transfected with 250 ng of STAT1-GFP along with 250 ng of ORF6 strep. 24 hours post-transfection, cells were induced for 1 h with 1000 U/ml Universal Type-I interferon (IFN). For RIG-I co-localization, HeLa cells were transfected with 250 ng of RIG-I Flag or MAVS Flag and 250 ng of ORF6 strep for 24 h. For TRIM25 studies during infection, A549 ACE2 cells were infected at 1 MOI. 6 hours post-infection cells were treated with MG132 (10 µM) for another 18 hours. The cells were fixed in PBS containing 4% formaldehyde at room temperature for 20 minutes after being twice rinsed with 1X PBS. After that, the cells were permeabilized for 10 minutes at room temperature using 1% Tween-20 in PBS. Following three 1X PBS washes, cells were incubated for two hours at room temperature (RT) in a blocking buffer containing 2% BSA in 1X PBS containing 0.3% Tween-20. This was followed by two PBS washes with wash buffer (PBS with 0.3% Tween 20). Using a 1:500 ratio, diluted primary antibodies in 50 µl PBS containing 0.3% Tween 20 and 0.5% BSA coverslips were incubated for three hours at room temperature. Cells were washed thrice with wash buffer followed by incubation with secondary antibody. After three rounds of washing with wash buffer, the cells were counter-stained for ten minutes at room temperature using 4',6-diamidino-2-phenylindole (DAPI). Coverslips were placed on a slide using antifade mounting material after being cleaned three times with PBS. Images were acquired using Zeiss 880 or Leica SP8 confocal microscope.

2.3.6 Quantitative RT PCR

Procedure is same as mentioned on point 1.3.12.

2.4 Results

2.4.1 Multiple SARS-CoV-2 proteins antagonize type-I IFN induction and signalling

We started the research with the aim of finding every SARS-CoV-2 protein that might antagonize type-I IFN induction. For that, at the beginning of the pandemic, we procured SARS-CoV-2 plasmids cloned in mammalian expression vector from Prof. Navan Krogan's lab and then we checked the expression of these plasmids. We observed that all the proteins expressed at variable levels. However, some proteins (NSP11, ORF3b, and ORF7b; mentioned inside the red box) did not give detectable bands (Figure 10 A), thus excluded from our subsequent screening. To identify SARS-CoV-2 proteins antagonizing the IFN induction pathway, we performed a dual luciferase assay. The principle of the assay involves co-transfecting HEK 293T cells with Firefly luciferase reporter plasmid luciferase where luciferase is driven by IFN promoter, PRLtK which constitutively expresses renilla luciferase and act as an internal control and plasmids expressing SARS-CoV-2 protein or empty vector. 24 hours later cells were transfected with poly (I:C), an inducer of RLR pathway, and 12 hours later cells were lysed to measure the luciferase activity (Figure 10B). We observed that, NSP 1, NSP5, 6, 7, 10, 13, 14, 15 and ORF6 showed >70% inhibition on IFNβ promoter activation (Figure 10C).

Next, we screened the SARS-CoV-2 proteins that antagonize the IFN signalling pathway. For that another dual luciferase assay was performed. Here, HEK 293T cells were co-transfected with Firefly luciferase reporter plasmid luciferase where luciferase is driven by ISG promoter, renilla luciferase expressing PRLtK and plasmids expressing SARS-CoV-2 protein or empty vector. 24 hours later cells were induced with universal IFN (1000 U/ml) and 12 hours later cells were lysed to measure the luciferase activity (Figure 10D). We observed that NSP1, 5, 13, & 14 and ORF6 showed more than 70% reduction on ISG promoter activation. In addition to the proteins listed above, a few other proteins also, albeit less successfully, blocked signaling (NSP7, NSP9, ORF9b) or IFN induction (NSP4, NSP8, NSP9, NSP12, N, E, M, ORF7a, ORF9b). So taken together, multiple SARS-CoV-2 proteins inhibited type I IFN pathway (both IFN induction and signalling pathway).

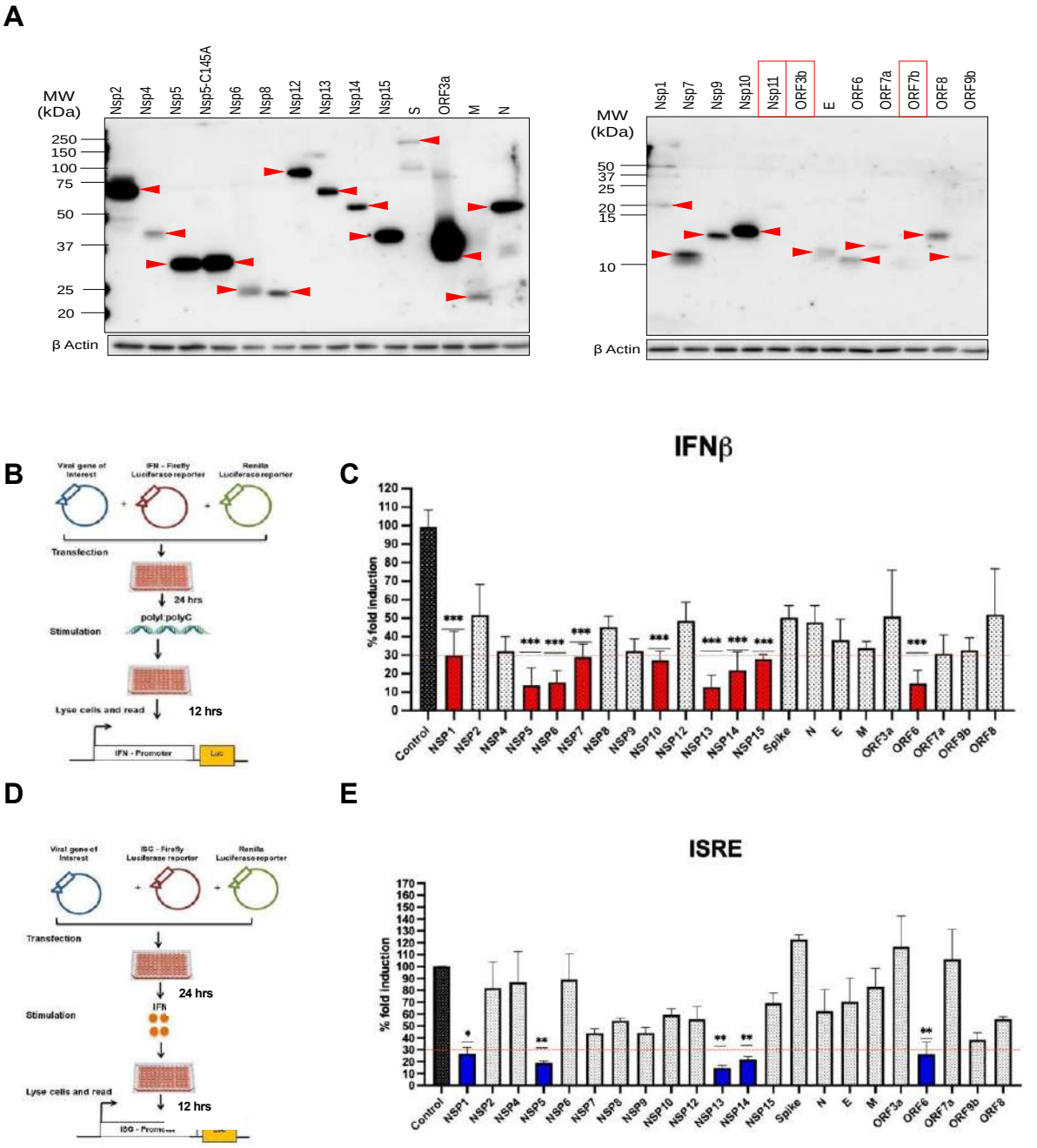

Figure 10: Screening SARS-CoV-2 proteins to identify antagonist of IFN induction and signalling pathway. A) Western blot analysis of SARS-CoV-2 genes cloned in a mammalian expression vector. B) Schematic representation of dual luciferase assay for the IFN induction pathway. C) Quantification of IFNβ dual luciferase assay of all SARS-CoV-2 proteins. D) Schematic representation of dual luciferase assay for the IFN signalling pathway. E) Quantification of ISG dual luciferase assay of all SARS-CoV-2 proteins. The schematic is adapted from *https://www.bmglabtech.com/dual-luciferase-reporter-assay-to-study-the-interferon-signalling-pathways-in-virology/* .

We compiled and compared data from earlier studies that used similar reporter-based techniques to screen for SARS-CoV-2 IFN antagonists in order to further support our findings (28-36). We observed that our findings largely corroborated with published studies (Figure 11 A & B). Furthermore, ORF6 is appeared as one of the strongest antagonist of both IFN induction and signalling pathway. So, we focused our subsequent study on ORF6.

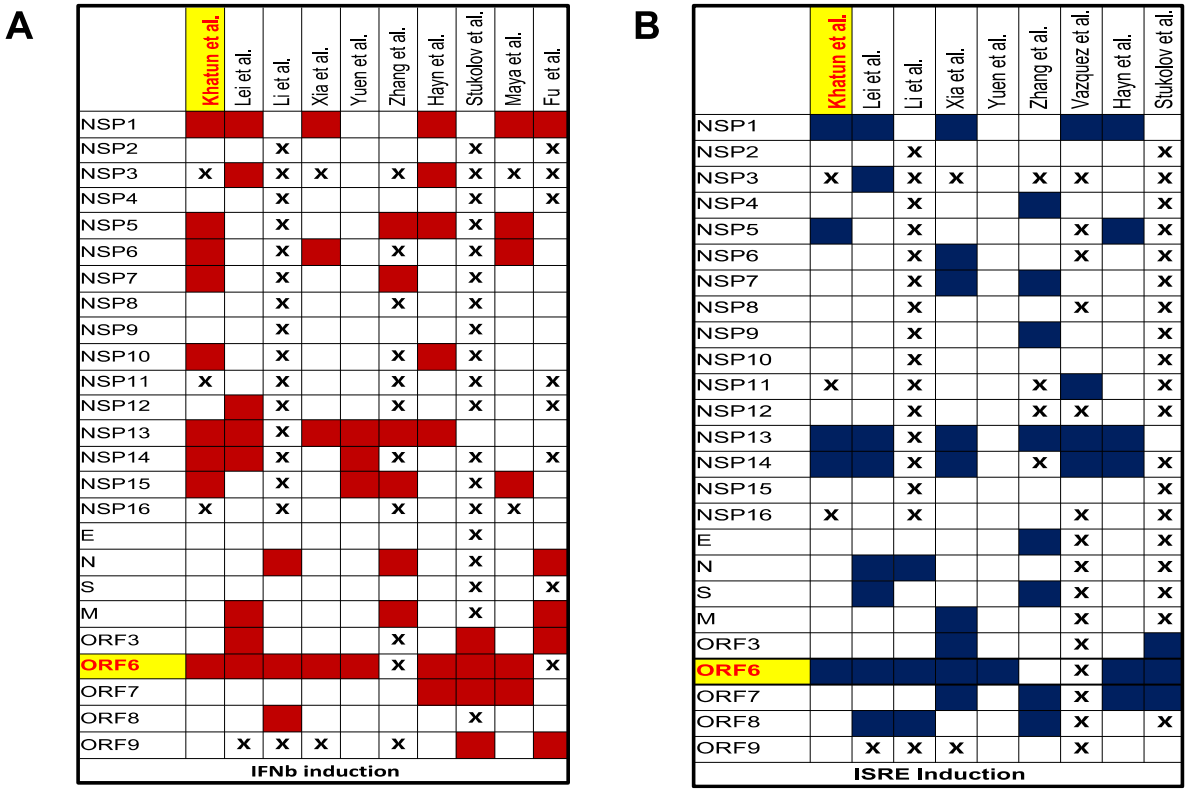

Figure 11: Comparing our IFN induction (A) and signalling (B) screening with published studies. Here, filled boxes represent proteins that were reported as antagonist, empty are not antagonists, and X represent they were not tested.

2.4. 2 ORF6 antagonizes innate immune pathway at various steps

Next, we examined ORF6's ability to inhibit IFN induction in the presence of a virus infection. We found that, in Sendai virus (SeV) infected cells, SARS-CoV-2 ORF6, in a dose-dependent way, suppressed the activation of IFNβ-Luciferase (Figure 12A). This was verified by assessing how ORF6 expression affected the amounts of IFNβ and ISG54 transcripts in SeV-infected cells using RT-PCR (Figure 12B). To dissect the steps of IFN induction pathway and identify specific target proteins, we performed dual luciferase assay where HEK 293T cells were co-transfected with different proteins of the IFN induction pathway as inducer along with reporter plasmids and ORF6. We observed that ORF6 inhibited IFNβ induced by RIG-I 2CARD,

MAVS, TBK1, IKKe, IRF3-5D (a constitutively active form of IRF3), and IRF7-CA (a constitutively active form of IRF7) to varying degrees, with the very prominent effect seen at the level of RIG-I (Figure 12 C-H). To further investigate this, we looked at how ORF6 interacted with important IFN induction and signaling mediators, including RIG-I, MAVS, STAT1, and STAT2, and discovered that ORF6 interacted with all of them except STAT1 (Figure 12 I). we corroborated this by performing immunofluorescence, and observed that ORF6 co-localizes with RIG-I and MAVS (Figure 12K) (MAVS images not shown here).

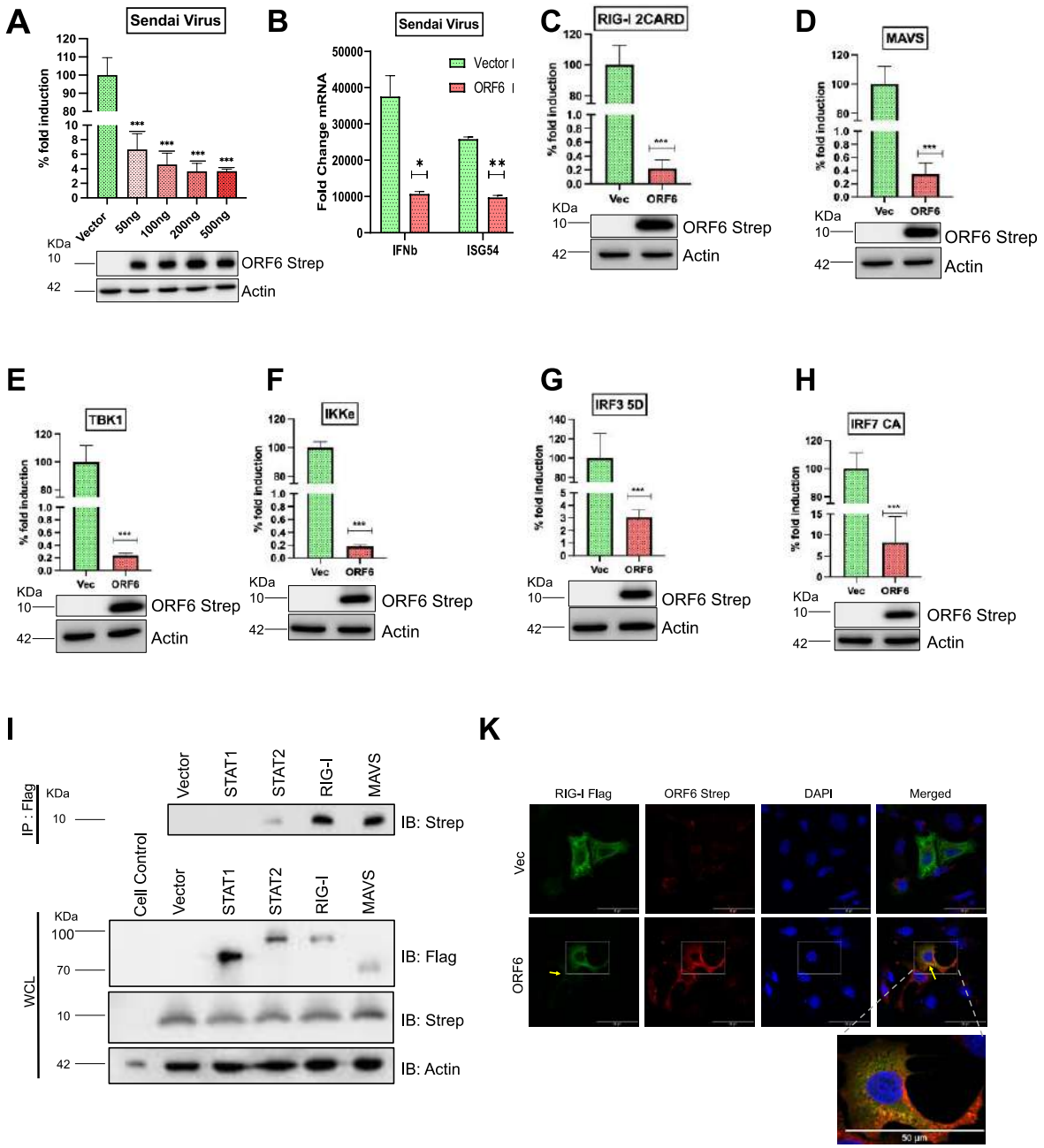

Figure 12: ORF6 inhibits IFN induction pathway at various steps. A) Effects of increasing ORF6 on activation of the IFNβ promoter. The dual luciferase assay principle is same as

described in figure 11B, except here cells were infected with Sendai virus (instead of poly (I:C) transfection). B) mRNA levels of IFNb and ISG54 were measured from total RNA from HEK293T cells transfected with ORF6 or empty vector followed by Sendai virus infection. C-H) Impact of SARS-CoV-2 ORF6 on activation of the IFNβ promoter when distinct IFN induction pathway inducer protein is present. HEK293T cells were co-transfected with IFNβ firefly reporter, renilla luciferase plasmid, empty vector or ORF6 and plasmids expressing RIG-I 2CARD (C), MAVS (D), TBK1 (E), IKke (F), IRF3 5D (G) and IRF7 CA (H) as inducer protein. 24 hours post transfection cells were lysed. I) Co-immunoprecipitation of ORF6 strep with STAT1 Flag, STAT2 Flag, RIG-I Flag, and MAVS Flag. Here anti-Flag antibody was used to pull-down proteins. K) Representative fluorescence of images of co-localization of ORF6 strep with RIG-I Flag.

Next, we tested the effect of ORF6 on nuclear translocation of transcription factors. For that, we looked at the nuclear translocation of IRF3 GFP upon SeV infection or STAT1 GFP nuclear translocation upon IFN treatment. We observed that ORF6 inhibited their nuclear translocation (Figure 13 A, B), suggesting that ORF6 inhibits nuclear translocation of key transcription factors of IFN induction and signaling pathway.

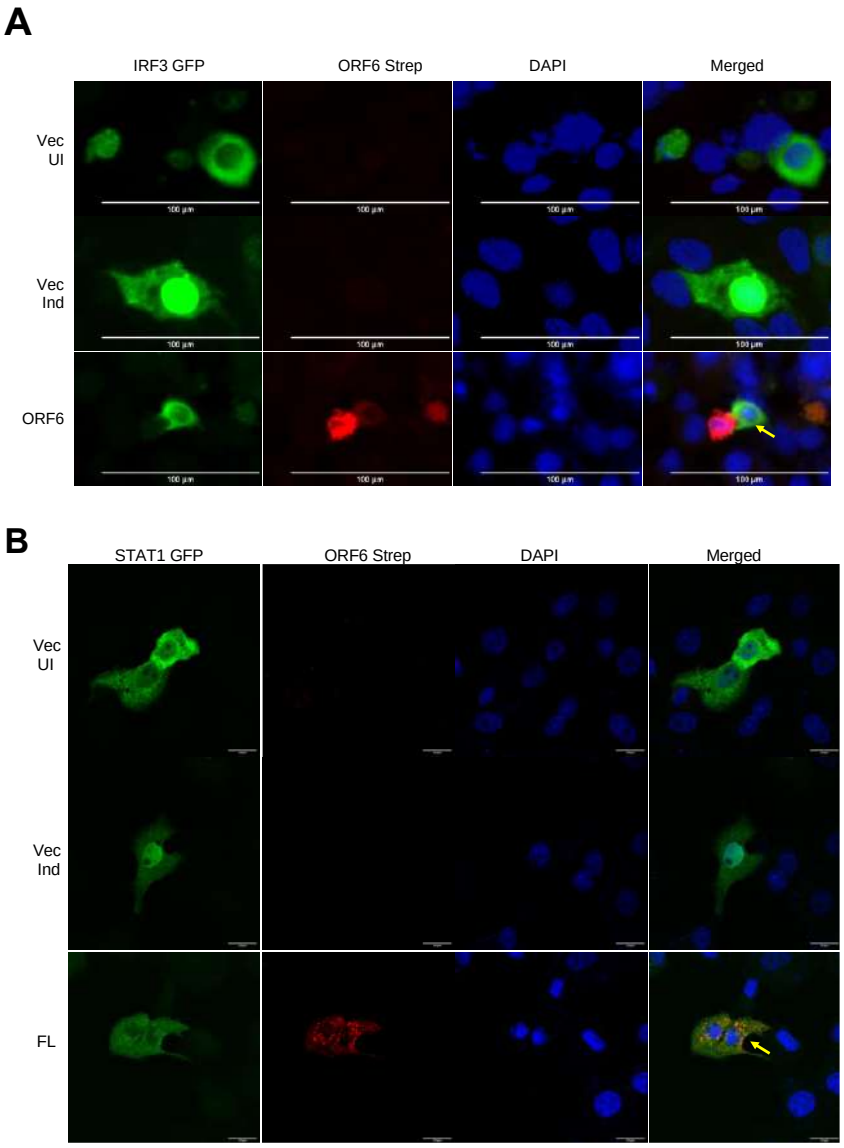

Figure 13: Nuclear translocation of IRF GFP and STAT1 in presence of ORF6. A) HEK 293T cells were co-transfected with IRF3 GFP and ORF6 strep or an empty vector for 24 hours, followed by SeV infection for 6 hours. B) HEK 293T cells were co-transfected with STAT1 GFP and ORF6 strep or an empty vector for 24 hours, followed by universal IFN treatment for 1 hours.

2.4.3 Mapping the domain of ORF6

SARS-CoV-2 ORF6 is a very small protein, consisting of 61 amino acids (35). Its ortholog is present in SARS-CoV and their the C-terminal domain is reported to be crucial for the IFN antagonism (37). This prompted us to map the domain of SARS-CoV-2 ORF6. For that we constructed a homology modelling, that showed its N- (M1-Q8) and C-terminal domain (N47-D61) remain in the cytoplasm, whereas the transmembrane domain (V9-E46) remain

embedded in the ER-golgi membrane (Figure 14A). we generated 3 deletion constructs, where N-terminal cytoplasmic domain is deleted (ΔN), C-terminal cytoplasmic domain is deleted (ΔC) (Figure 14B), and both N-terminal cytoplasmic domain and transmembrane domain is deleted (C-term). C-term construct failed to give detectable band, thus excluded from our subsequent studies. Using the luciferase reporter assay, we examined the ability of ORF6-specific domain deletion constructs to prevent IFN and ISG induction. It was observed that the ability of ΔC constructs to suppress IFN induction and subsequent signaling was considerably diminished (Figure 14 C, D). In comparison, ΔN was still effective in mitigating IFN induction pathway activation. Furthermore, this activity was validated in presence of RIG-I 2CARD and IRF3 5D as inducer (Figure 14 E, F), suggesting that C-terminal cytoplasmic domain is crucial for IFN antagonism. Next, we tested the effect of domain deletion on IRF3 GFP nuclear translocation upon SeV infection. We observed that similar to full-length (FL), ΔN could successfully inhibit the nuclear translocation of IRF3 GFP. However, ΔC lost is this antagonism (Figure 15). This data potentiates our claim, that C-terminal cytoplasmic domain of ORF6 is crucial for antagonizing the IFNβ promoter activation.

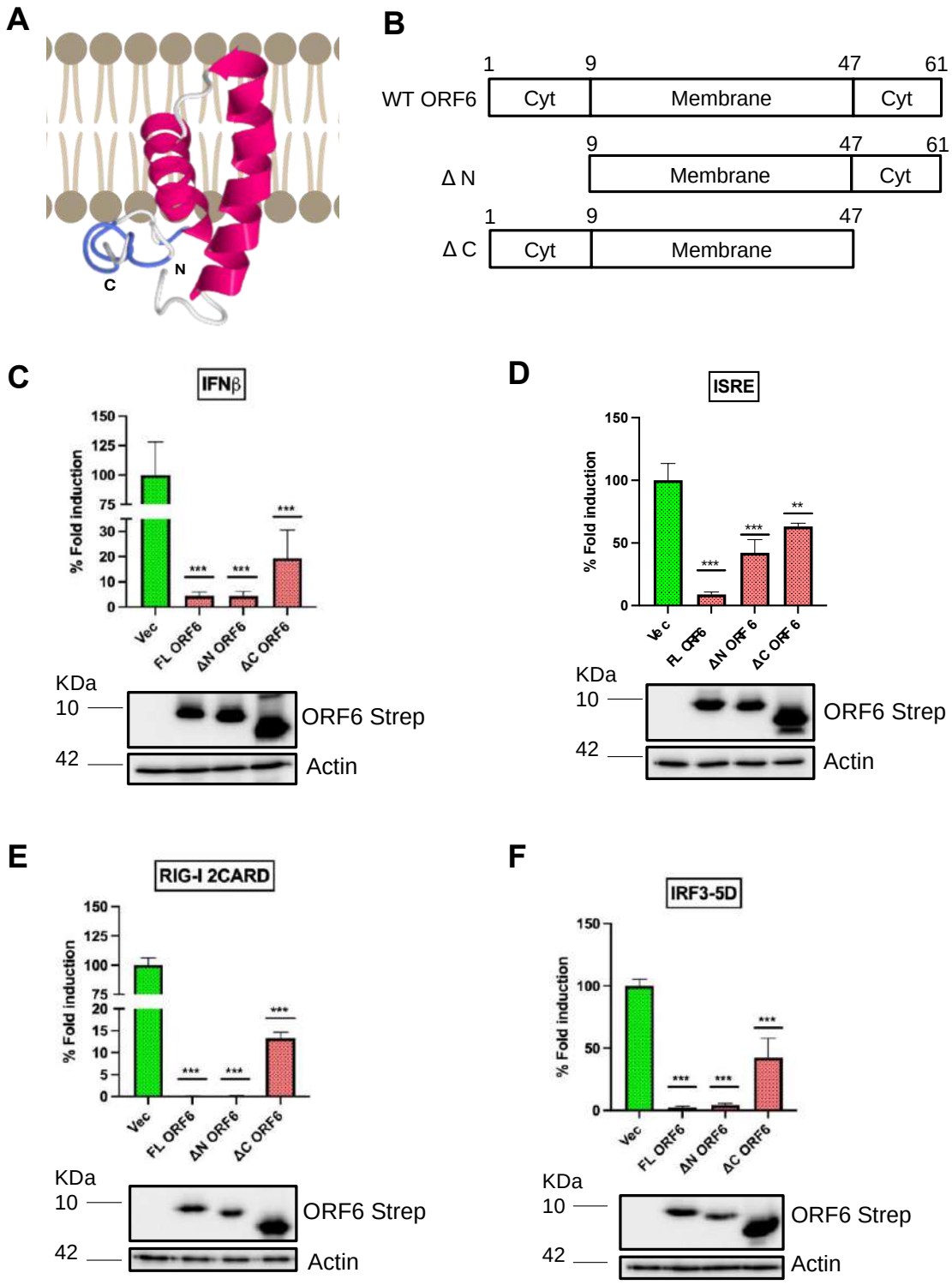

Figure 14: Mapping the domain of ORF6. A) Three-dimensional predicted model structure of ORF6. Prediction was done using I-TASSER (Iterative Threading Assembly Refinement) standalone software version 5, which was visualized using Jmol 14.32. The final image was made using Biorender.com. B) Schematic representation of the domain structure of ORF6 and involved amino acids. WT: wild type, ΔN: N-terminal cytoplasmic domain is deleted, and ΔC: C-terminal domain is deleted. C, D) Dual-luciferase assay depicting the effect of full length

(FL) and deletions of ORF6 on IFNβ (**C**) and ISRE (**D**) promoter activation. The principle of the assay is described in figure 10B and 10D respectively. E, F) Dual-luciferase assay depicting the effect of full length (FL) and deletions of ORF6 on IFNβ promoter activation in presence of RIG-I 2CARD (E) and IRF3 5D (F). The principle of the assay is same as figure 12 C-H.

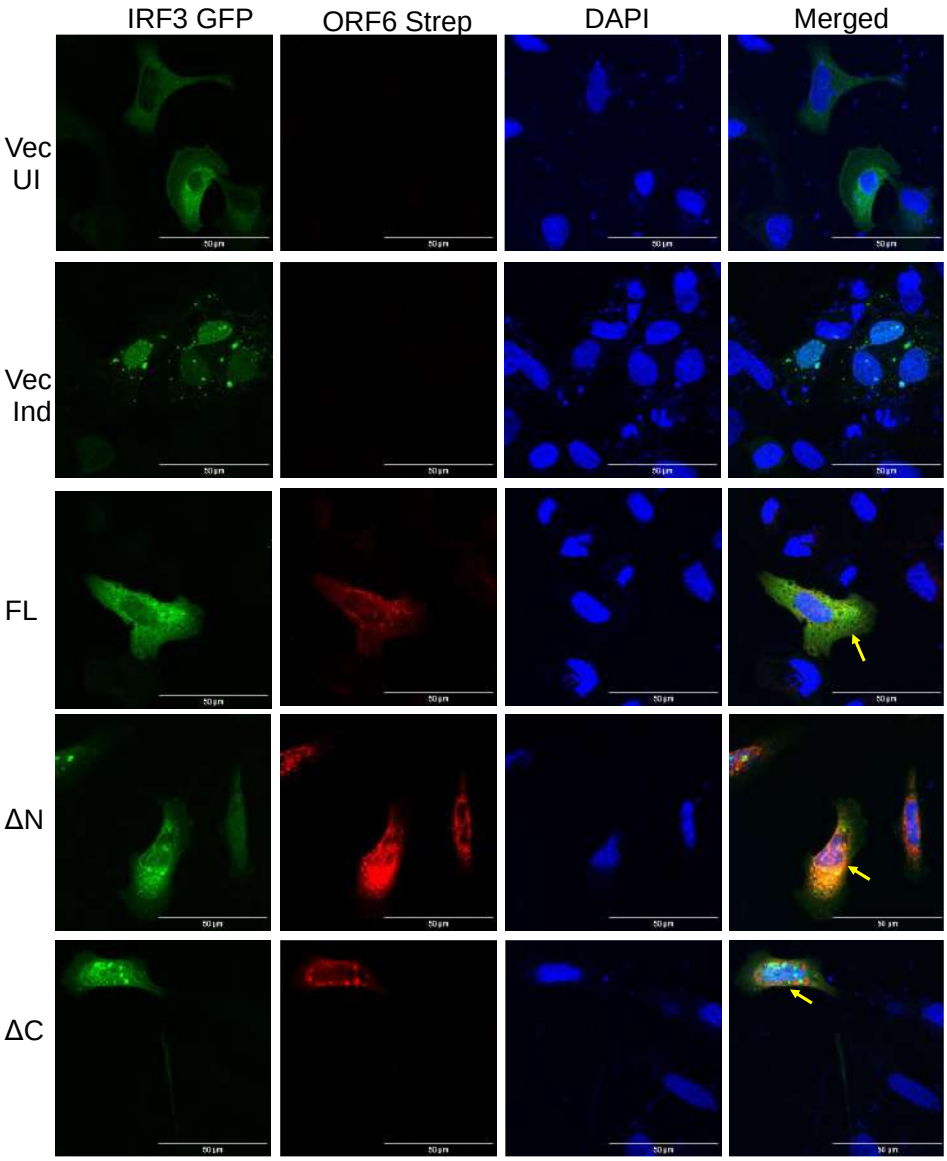

Figure 15: Effect of deletion constructs of ORF6 on IRF3 GFP nuclear translocation.

2.4.4 Mapping the amino acids of ORF6

Next, we mapped the amino acids present in C-terminal cytoplasmic domain crucial for IFN antagonism. We created four alanine scanning mutations that are four amino acids long and have two amino acid overlaps, called called ORF6 M1 (aa 52–55), M2 (aa 54–57), and M3 (aa 56–59) and M4 (58–61) (Fig. 16A). Next, we investigated these mutants' ability to interfere with the IFNβ induction pathway, which is stimulated by RIG-I 2CARD and IRF3-5D. we

observed all the mutants from M1 to M3 progressively lost their IFN antagonism against both RIG-I and IRF3, with ORF6 M3 and M4 showing maximum loss (Figure 16 B, C). interestingly, all the mutants were equally ineffective in inhibiting IFN signalling pathway (Figure 16D). These data suggest that, amino acids 52-61 are crucial for the IFN antagonism.

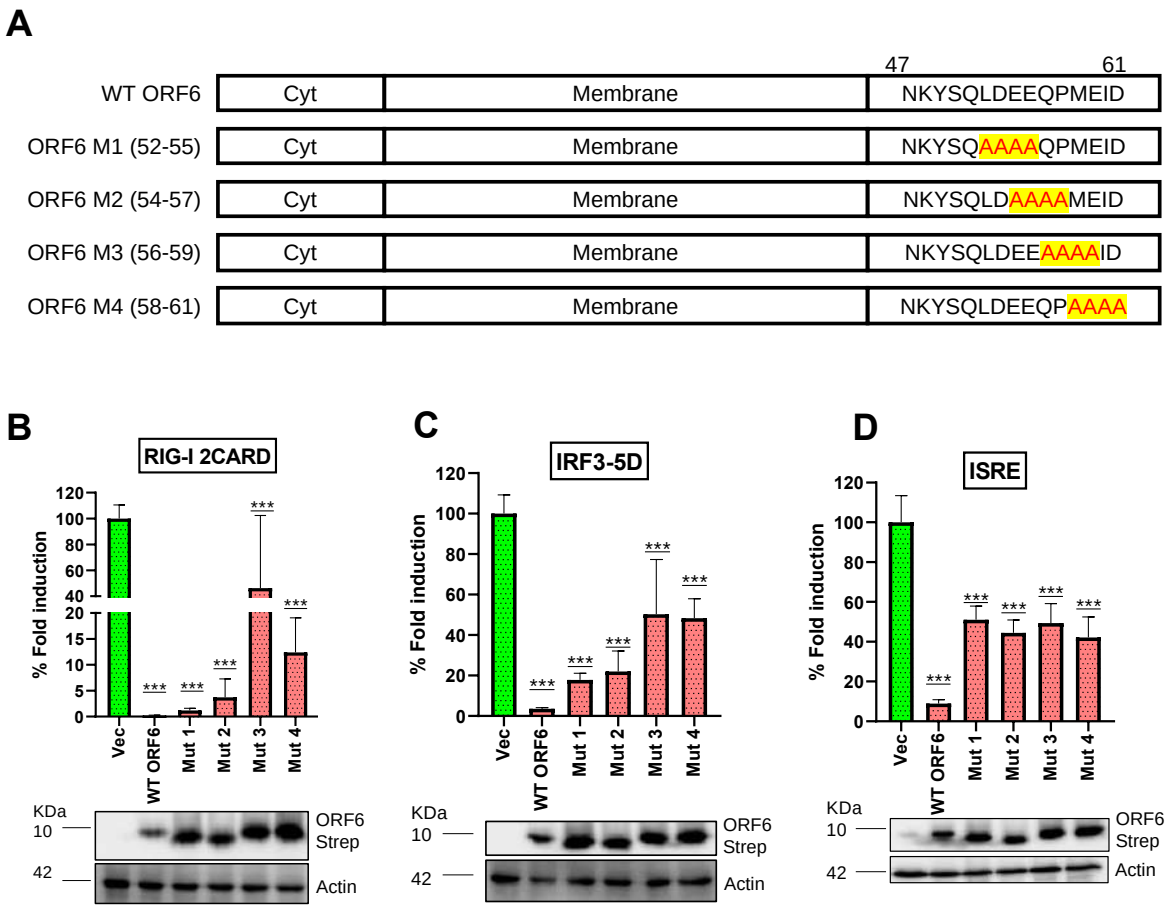

Figure 16: Mapping the amino acids crucial for IFN antagonism. A) Schematic representation of 4 mutant constructs. Here WT is wild type. In that mutants, amino acids are replaced with alanine (highlighted, amino acids positions are mentioned inside bracket). B, C) Effect of mutant constructs on RIG-I 2CARD (B) and IRF3-5D (C) induced IFN pathway activation. The principle of the assay is mentioned in figure 12 C-H. D) Dual-luciferase assay depicting the effect of full length (FL) and mutants of ORF6 ISRE promoter activation. The principle of the assay is described in figure 10D.

2.4.5 ORF6 reduces the K63-ubiquitinated RIG-I

Previously we have seen that ORF6 inhibits RIG-I mediated IFN induction pathway and it directly interacts with RIG-I. so explored the regulation of ORF6 on RIG-I. In that context, we checked whether the interaction with RIG-I is affected in presence of RIG-I, because we have observed loss of IFN antagonism during RIG-I 2CARD mediated IFN activation. Surprisingly, we did not observe any loss in interaction in case of deletion constructs (Figure 17A). So evaluated the effect of ORF6 on RIGI-I mRNA level, which revealed only 50% reduction (Figure 17B), and this fails to explain such strong reduction at RIG-I mediated IFN induction. So, we explored the effect on RIG-I post-translational modification. RIG-I is known to undergo K63-linked ubiquitination. It is added by E3 ligase TRIM25 (38). We performed immunoprecipitation and observed that in ORF6 FL and ΔN reduced K63-ubiquitinated RIG-I level; however, in case of ΔC, it has lost the ability to reduce this ubiquitination and K63-ubiquitinated levels (Figure 17 C, D). Next, we explored the effect of ORF6 on TRIM25 stability at the protein level and observed that TRIM25 protein is reduced in presence of FL ORF6, which is rescued in case of ΔC (Figure 18A). Viruses frequently employ the cellular proteasome machinery to target innate immune signaling mediators for degradation (39). Thus, we tested the subsequent changes on TRIM25 upon adding proteasomal inhibitor, MG132. We observed that ORF6 reduced TRIM25 level, which is rescued upon MG132 treatment. Concomitantly, it rescued corresponding RIG-I ubiquitination (Figure 18 B & C). These data suggest that ORF6 targets TRIM25 for proteasomal degradation and thus reduce K63-linked RIG-I ubiquitination.

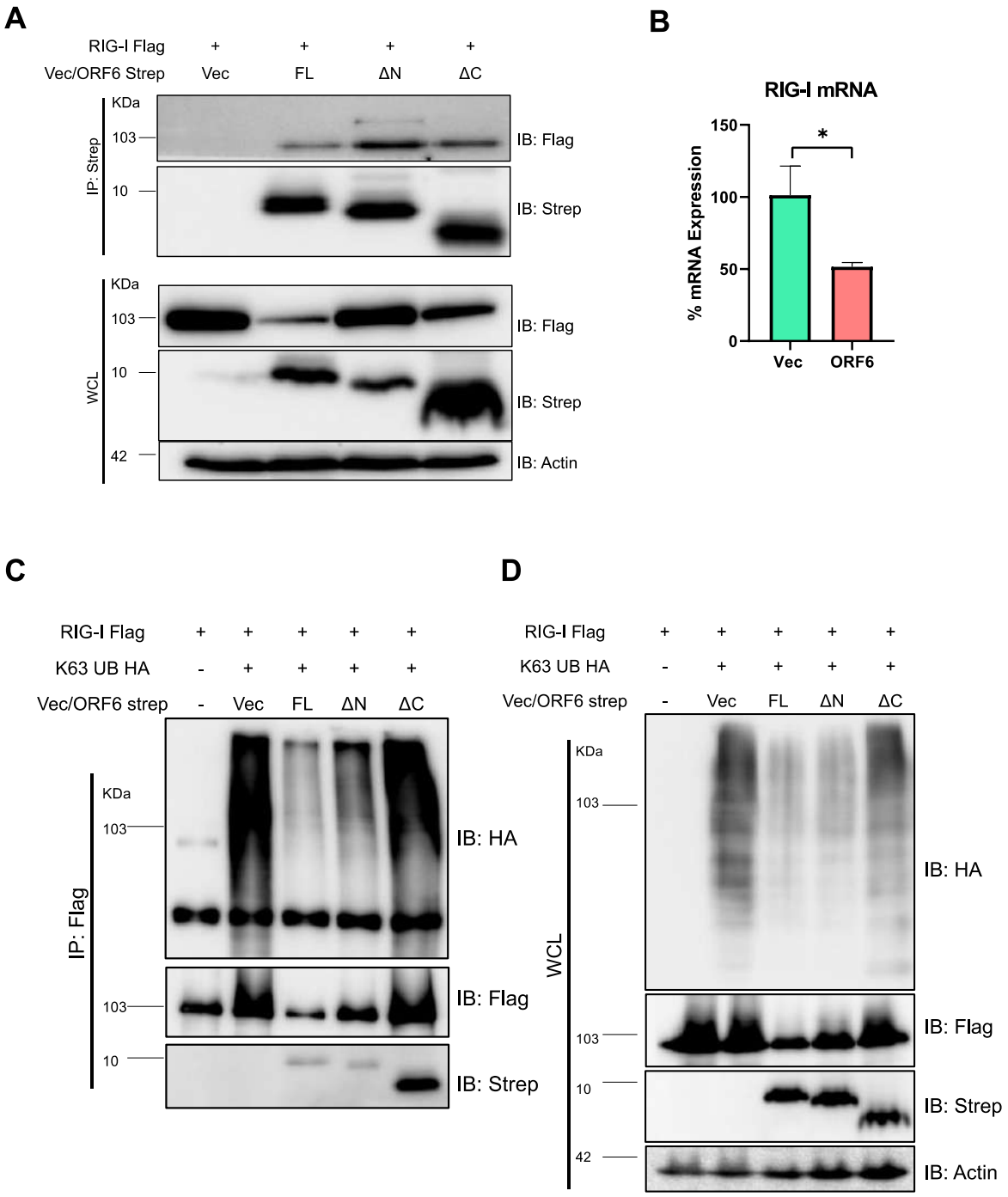

Figure 17: ORF6 reduces RIG-I ubiquitination. A) Immunoprecipitation of RIG-I Flag with full-length (FL) pr deletion constructs of ORF6 strep. Immunoprecipitation was performed using anti-strep antibody. B) Effect of ORF6 on RIG-I RNA level. C&D) Western blot analysis with cell lysates from HEK293T cells co-transfected with RIG-I Flag, K63-linked UB HA, and different deletions of ORF6-strep or empty vector. Cell lysates were either directly assessed as WCL (**D**) or incubated overnight with anti-Flag antibody followed by analysis as IP fraction (**C**) and probed with indicated antibodies

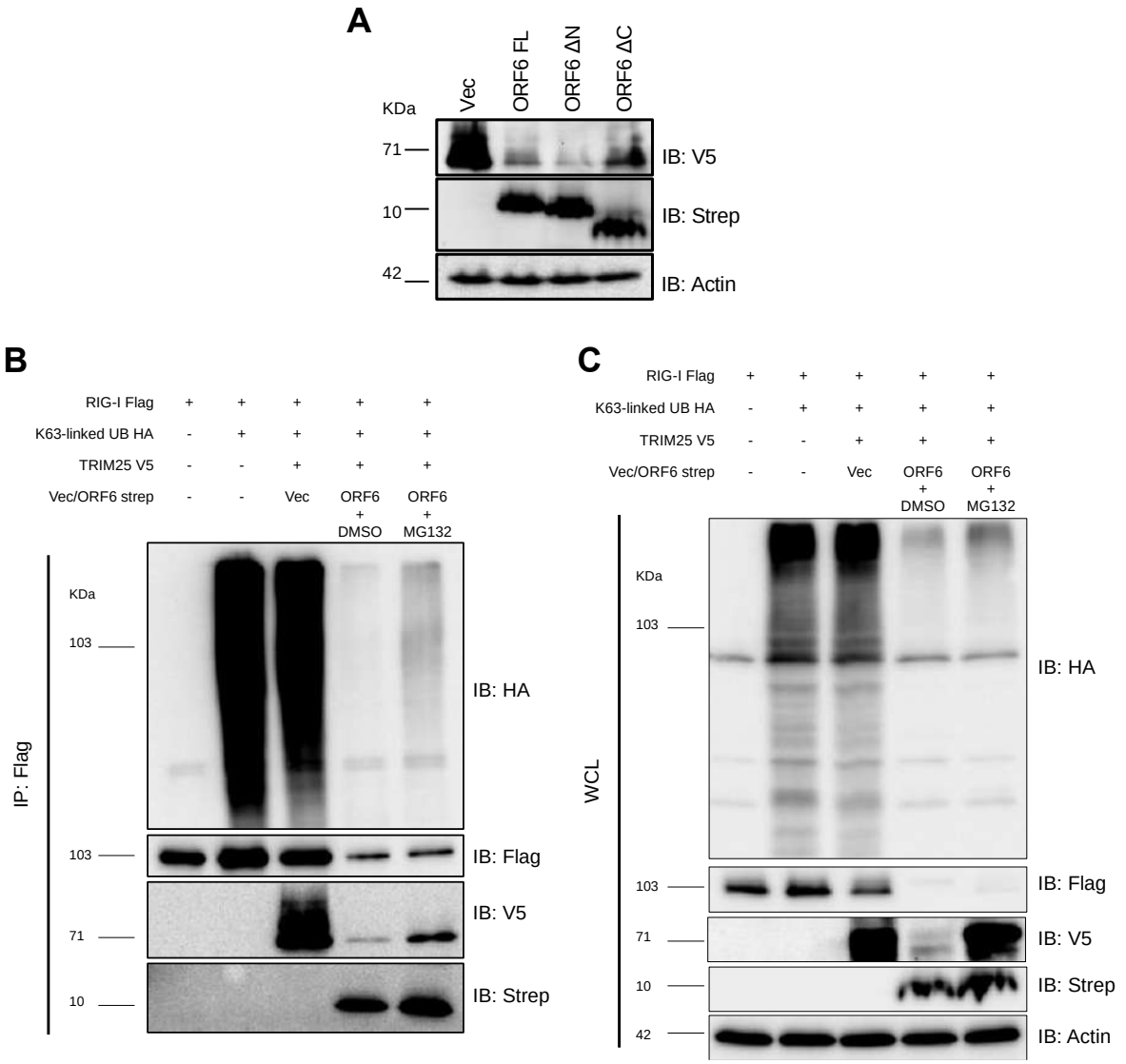

Figure 18: Checking the effect of ORF6 on TRIM25 stability. A) Western blot analysis with cell lysates from HEK 293 T cells co-transfected with TRIM25 V5 and empty vector or strep-tagged ORF6 (FL or ΔN or ΔC) for 48 h. B, C) Western blot analysis with cell lysates from HEK293T cells co-transfected with RIG-I Flag, K63-linked UB HA, TRIM25 V5 and empty vector or ORF6-strep for 24 h, followed by MG132 treatment (10 μM) for 12 h. Cell lysates were either directly assessed as WCL (C) or incubated overnight with anti-Flag antibody followed by analysis as IP fraction (B) and probed with indicated antibodies

2.4.6 SARS-CoV-2 infection targets TRIM25 for proteasomal degradation

Next, we validated the TRIM25 degradation during SARS-CoV-2 infection. We observed that during infection in HEK ACE2, TRIM25 levels are reduced, which is rescued after MG132 treatment. We quantified the same here. Since MG132 treatment has rescued TRIM25 protein level, it should rescue the IFN pathway as well. Thus, we looked the transcript level of IFN , and ISGs.

We found their levels were increased upon MG132 treatment. These data suggest that TRIM25 is targeted for proteasomal degradation during SARS-CoV-2 infection. Next we wanted to confirm our finding in other cell line as well. For that we did infection in A549 ACE2 in presence and absence of MG132 and performed WB and immunofluorescence. We observed, during infection TRIM25 level was reduced which was rescued upon MG132 treatment. Representative immunofluorescence and quantification also shows the same, i.e., MG132 treatment has rescued the TRIM25 level. Corroborating our previous statement that TRIM25 is targeted for proteasomal degradation.

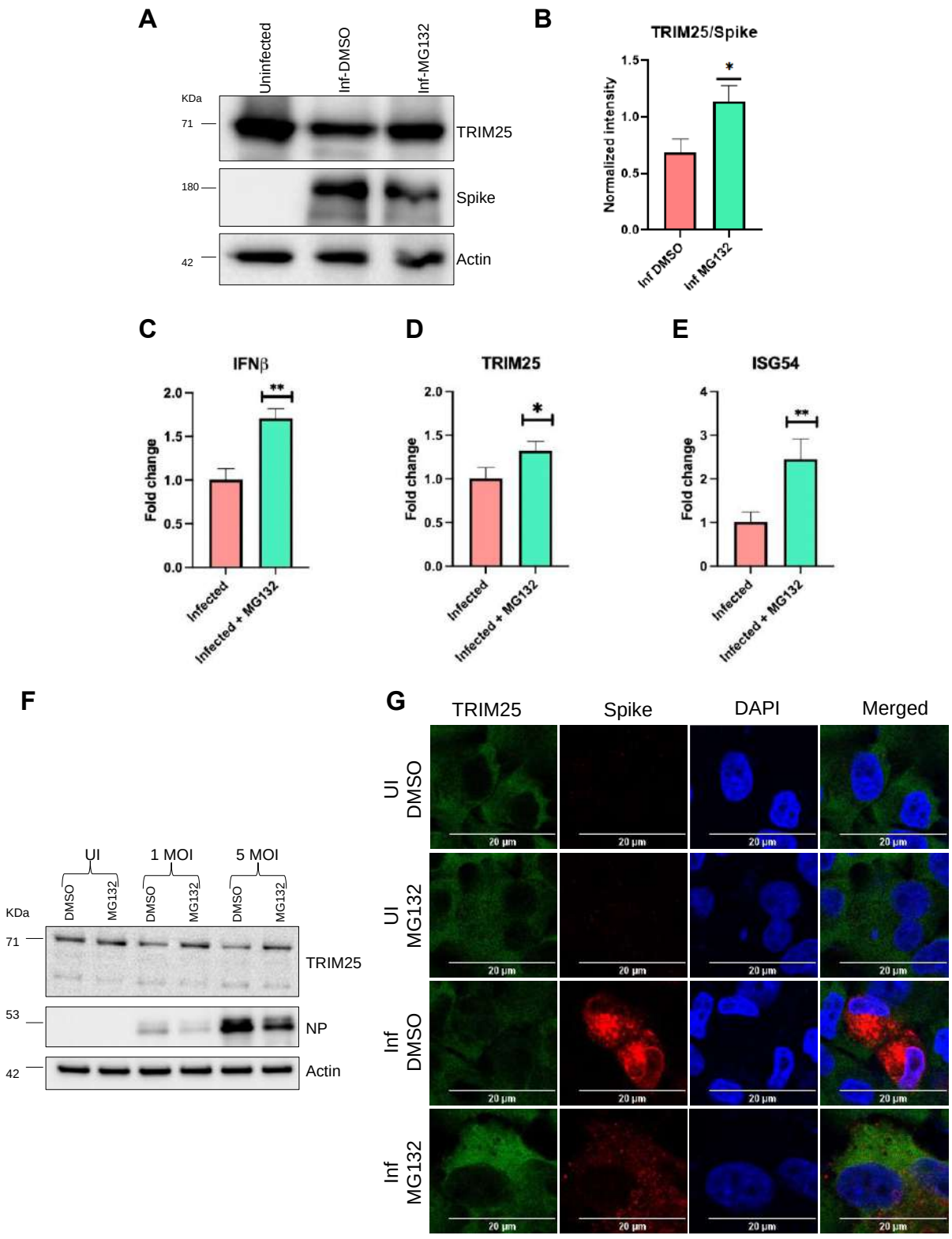

Figure 19: TRIM25 is targeted for proteasomal degradation during SARS-CoV-2 infection. A) Western blot analysis with cell lysates from HEK-ACE2 cells infected with SARS-CoV-2 at 1 MOI. 6 hours post-infection, cells were treated with MG132 (10 μM) for 18 hours followed by harvesting the cell lysates. B) Quantification of fluorescence intensity of TRIM25 and Spike from WB. C-E) mRNA level of IFNβ (C), TRIM25 (D), and ISG54 (E). Experiment outline is same as described in panel A.F

& G) EB analysis and immunofluorescence images of TRIM25 during SARS-CoV-2 infection in A549 ACE2. cells infected with SARS-CoV-2 at 1 MOI. 6 hour post-infection, cells were treated with MG132 (10 μM) for 18 hours followed by harvesting the cell lysates for WB or fixation for IFA.

2.5 Statistical Analysis

All numerical data of bar graph were analyzed and plotted using GraphPad Prism v8.0.2. Statistical significance was calculated using a *t* test with Bonferroni corrections for multiple comparisons (wherever necessary). The P values were indicated as $*P < 0.05$; $**P < 0.01$; $***P < 0.001$; ns = not significant. Error bars represent mean + standard error.

2.6 Discussion

The pathogenesis of COVID-19 is facilitated by the virus's ability to evade and counter the host cellular immunity during SARS-CoV-2 infection. We investigated the possible ability of various SARS-CoV-2 proteins to counteract the host's innate immune system and discovered that type-I Interferon (IFN) activation and subsequent IFN signaling were diminished by the ORF6 protein. Our results further supported earlier observations that ORF6 inhibits IFN production and signaling by blocking the nuclear translocation of IRF3 and STAT1. Here, we demonstrate how ORF6 directly interacts with RIG-I and lowers the amount of K63-linked ubiquitinated RIG-I, hence blocking downstream type-I IFN induction and signaling. This is related to the observation of ORF6-mediated targeting of TRIM25, an E3 ligase, for proteasomal destruction during SARS-CoV-2 infection. The amino acid residues 52–61 in ORF6's C-terminal cytoplasmic tail are specifically responsible for its type-IIFN antagonistic action. Overall, we shed light on the several ways that the viral ORF6 protein functions to prevent type-I IFN production and signaling in SARS-CoV-2.

2.7 Impact of the research in the advancement of knowledge or benefit to mankind

SARS-CoV-2 infection is associated with interreference of early immune response, diminish the interferon (IFN) production, followed by exacerbated inflammatory immune response. This often results in cytokine storm. Thus, it needed detailed understanding of this early immune evasion. So, we screened all SARS-CoV-2 proteins to identify the antagonist of the innate immune pathway. We observed that along with many other proteins, ORF6 showed a very potent antagonism of IFN pathway. We elucidated the mechanism of this antagonism and showed that it inhibits K63-linked ubiquitinated RIG-I level, the active form of RIG-I and crucial for mediating the IFN induction, by targeting the corresponding E3 ligase TRIM25 for

proteasomal degradation. In summary, we offer novel perspectives on how the unique functions of the viral ORF6 protein enable SARS-CoV-2 to interfere with type-I IFN production and signaling. Finally, ORF6 as an accessory protein of SARS-CoV-2, which may be dispensable for viral replication, can be removed from the viral genome to engineer attenuated strains, potentially useful as vaccines.

3. Literature reference.

1. Lieberman NAP, Peddu V, Xie H, Shrestha L, Huang ML, Mears MC, et al. In vivo antiviral host transcriptional response to SARS-CoV-2 by viral load, sex, and age. PLoS Biol. 2020;18(9):e3000849.
2. Grant RA, Morales-Nebreda L, Markov NS, Swaminathan S, Querrey M, Guzman ER, et al. Circuits between infected macrophages and T cells in SARS-CoV-2 pneumonia. Nature. 2021;590(7847):635-41.
3. Xiong Y, Liu Y, Cao L, Wang D, Guo M, Jiang A, et al. Transcriptomic characteristics of bronchoalveolar lavage fluid and peripheral blood mononuclear cells in COVID-19 patients. Emerg Microbes Infect. 2020;9(1):761-70.
4. Zhou Z, Ren L, Zhang L, Zhong J, Xiao Y, Jia Z, et al. Heightened Innate Immune Responses in the Respiratory Tract of COVID-19 Patients. Cell Host Microbe. 2020;27(6):883-90 e2.
5. Rivera B, Leyva A, Portela MM, Moratorio G, Moreno P, Duran R, et al. Quantitative proteomic dataset from oro- and naso-pharyngeal swabs used for COVID-19 diagnosis: Detection of viral proteins and host's biological processes altered by the infection. Data Brief. 2020;32:106121.
6. Akgun E, Tuzuner MB, Sahin B, Kilercik M, Kulah C, Cakiroglu HN, et al. Proteins associated with neutrophil degranulation are upregulated in nasopharyngeal swabs from SARS-CoV-2 patients. PLoS One. 2020;15(10):e0240012.
7. Maras JS, Sharma S, Bhat A, Rooge S, Aggrawal R, Gupta E, et al. Multi-omics analysis of respiratory specimen characterizes baseline molecular determinants associated with SARS-CoV-2 outcome. iScience. 2021;24(8):102823.
8. Case JB, Bailey AL, Kim AS, Chen RE, Diamond MS. Growth, detection, quantification, and inactivation of SARS-CoV-2. Virology. 2020;548:39-48.
9. Liesenborghs L, Spriet I, Jochmans D, Belmans A, Gyselinck I, Teuwen LA, et al. Itraconazole for COVID-19: preclinical studies and a proof-of-concept randomized clinical trial. EBioMedicine. 2021;66:103288.
10. Du S, Cao Y, Zhu Q, Yu P, Qi F, Wang G, et al. Structurally Resolved SARS-CoV-2 Antibody Shows High Efficacy in Severely Infected Hamsters and Provides a Potent Cocktail Pairing Strategy. Cell. 2020;183(4):1013-23 e13.
11. Chan JF, Zhang AJ, Yuan S, Poon VK, Chan CC, Lee AC, et al. Simulation of the Clinical and Pathological Manifestations of Coronavirus Disease 2019 (COVID-19) in a Golden Syrian Hamster Model: Implications for Disease Pathogenesis and Transmissibility. Clin Infect Dis. 2020;71(9):2428-46.

12. Bushman FD, Malani N, Fernandes J, D'Orso I, Cagney G, Diamond TL, et al. Host cell factors in HIV replication: meta-analysis of genome-wide studies. PLoS Pathog. 2009;5(5):e1000437.
13. Gromer S, Arscott LD, Williams CH, Jr., Schirmer RH, Becker K. Human placenta thioredoxin reductase. Isolation of the selenoenzyme, steady state kinetics, and inhibition by therapeutic gold compounds. J Biol Chem. 1998;273(32):20096-101.
14. Holmgren A, Bjornstedt M. Thioredoxin and thioredoxin reductase. Methods Enzymol. 1995;252:199-208.
15. Sido B, Giese T, Autschbach F, Lasitschka F, Braunstein J, Meuer SC. Potential role of thioredoxin in immune responses in intestinal lamina propria T lymphocytes. Eur J Immunol. 2005;35(2):408-17.
16. Roder C, Thomson MJ. Auranofin: repurposing an old drug for a golden new age. Drugs R D. 2015;15(1):13-20.
17. Schenk H, Vogt M, Droge W, Schulze-Osthoff K. Thioredoxin as a potent costimulus of cytokine expression. J Immunol. 1996;156(2):765-71.
18. Tufan A, Avanoglu Guler A, Matucci-Cerinic M. COVID-19, immune system response, hyperinflammation and repurposing antirheumatic drugs. Turk J Med Sci. 2020;50(SI-1):620-32.
19. Crawford KHD, Eguia R, Dingens AS, Loes AN, Malone KD, Wolf CR, et al. Protocol and Reagents for Pseudotyping Lentiviral Particles with SARS-CoV-2 Spike Protein for Neutralization Assays. Viruses. 2020;12(5).
20. V'Kovski P, Kratzel A, Steiner S, Stalder H, Thiel V. Coronavirus biology and replication: implications for SARS-CoV-2. Nat Rev Microbiol. 2021;19(3):155-70.
21. Li X, Lidsky PV, Xiao Y, Wu CT, Garcia-Knight M, Yang J, et al. Ethacridine inhibits SARS-CoV-2 by inactivating viral particles. PLoS Pathog. 2021;17(9):e1009898.
22. Hou YJ, Okuda K, Edwards CE, Martinez DR, Asakura T, Dinnon KH, 3rd, et al. SARS-CoV-2 Reverse Genetics Reveals a Variable Infection Gradient in the Respiratory Tract. Cell. 2020;182(2):429-46 e14.
23. Sa Ribero M, Jouvenet N, Dreux M, Nisole S. Interplay between SARS-CoV-2 and the type I interferon response. PLoS Pathog. 2020;16(7):e1008737.
24. Coronaviridae Study Group of the International Committee on Taxonomy of V. The species Severe acute respiratory syndrome-related coronavirus: classifying 2019-nCoV and naming it SARS-CoV-2. Nat Microbiol. 2020;5(4):536-44.
25. Li JY, Zhou ZJ, Wang Q, He QN, Zhao MY, Qiu Y, et al. Innate Immunity Evasion Strategies of Highly Pathogenic Coronaviruses: SARS-CoV, MERS-CoV, and SARS-CoV-2. Front Microbiol. 2021;12:770656.
26. Gordon DE, Jang GM, Bouhaddou M, Xu J, Obernier K, White KM, et al. A SARS-CoV-2 protein interaction map reveals targets for drug repurposing. Nature. 2020;583(7816):459-68.
27. Versteeg GA, Rajsbaum R, Sanchez-Aparicio MT, Maestre AM, Valdiviezo J, Shi M, et al. The E3-ligase TRIM family of proteins regulates signaling pathways triggered by innate immune pattern-recognition receptors. Immunity. 2013;38(2):384-98.
28. Lei X, Dong X, Ma R, Wang W, Xiao X, Tian Z, et al. Activation and evasion of type I interferon responses by SARS-CoV-2. Nat Commun. 2020;11(1):3810.
29. Xia H, Cao Z, Xie X, Zhang X, Chen JY, Wang H, et al. Evasion of Type I Interferon by SARS-CoV-2. Cell Rep. 2020;33(1):108234.

30. Fu YZ, Wang SY, Zheng ZQ, Yi H, Li WW, Xu ZS, et al. SARS-CoV-2 membrane glycoprotein M antagonizes the MAVS-mediated innate antiviral response. Cell Mol Immunol. 2021;18(3):613-20.
31. Hayn M, Hirschenberger M, Koepke L, Nchioua R, Straub JH, Klute S, et al. Systematic functional analysis of SARS-CoV-2 proteins uncovers viral innate immune antagonists and remaining vulnerabilities. Cell Rep. 2021;35(7):109126.
32. Li JY, Liao CH, Wang Q, Tan YJ, Luo R, Qiu Y, et al. The ORF6, ORF8 and nucleocapsid proteins of SARS-CoV-2 inhibit type I interferon signaling pathway. Virus Res. 2020;286:198074.
33. Shemesh M, Aktepe TE, Deerain JM, McAuley JL, Audsley MD, David CT, et al. Correction: SARS-CoV-2 suppresses IFNbeta production mediated by NSP1, 5, 6, 15, ORF6 and ORF7b but does not suppress the effects of added interferon. PLoS Pathog. 2021;17(12):e1010146.
34. Stukalov A, Girault V, Grass V, Karayel O, Bergant V, Urban C, et al. Multilevel proteomics reveals host perturbations by SARS-CoV-2 and SARS-CoV. Nature. 2021;594(7862):246-52.
35. Yuen CK, Lam JY, Wong WM, Mak LF, Wang X, Chu H, et al. SARS-CoV-2 nsp13, nsp14, nsp15 and orf6 function as potent interferon antagonists. Emerg Microbes Infect. 2020;9(1):1418-28.
36. Zhang Q, Chen Z, Huang C, Sun J, Xue M, Feng T, et al. Severe Acute Respiratory Syndrome Coronavirus 2 (SARS-CoV-2) Membrane (M) and Spike (S) Proteins Antagonize Host Type I Interferon Response. Front Cell Infect Microbiol. 2021;11:766922.
37. Chan JF, Kok KH, Zhu Z, Chu H, To KK, Yuan S, et al. Genomic characterization of the 2019 novel human-pathogenic coronavirus isolated from a patient with atypical pneumonia after visiting Wuhan. Emerg Microbes Infect. 2020;9(1):221-36.
38. Gack MU, Shin YC, Joo CH, Urano T, Liang C, Sun L, et al. TRIM25 RING-finger E3 ubiquitin ligase is essential for RIG-I-mediated antiviral activity. Nature. 2007;446(7138):916-20.
39. Gao G, Luo H. The ubiquitin-proteasome pathway in viral infections. Can J Physiol Pharmacol. 2006;84(1):5-14.